Geophys. J. Int. (2001) **145,** 401–422

NRM intensity of altered oceanic basalts across the MAR (21°N, 0–1.5 Ma): a record of geomagnetic palaeointensity variations?

Morgane Ravilly,[1] Hélène Horen,[2] Mireille Perrin,[3] Jérôme Dyment,[1] Pascal Gente[1] and Hervé Guillou[4]

[1] *Institut Universitaire Européen de la Mer, Université de Bretagne Occidentale, Plouzané, France. E-mail: jerome@sdt.univ-brest.fr*
[2] *Laboratoire de Géologie de l'Ecole Normale Supérieure de Paris, Paris, France*
[3] *Laboratoire de Géophysique, Tectonique et Sédimentologie, CNRS et Université de Montpellier* II, *Montpellier, France*
[4] *Laboratoire des Sciences du Climat et de l'Environnement, Gif-sur-Yvette, France*

Accepted 2000 November 22. Received 2000 November 22; in original form 1999 December 22

SUMMARY

During cruise Tammar (May 1996) of R/V Nadir and submersible Nautile, 66 basaltic rock samples were collected along two long cross-sections encompassing the oceanic crust between 0 and 1.5 Myr at the centre of the mid-Atlantic ridge segment located at 21°N. This dense sampling provides a means to investigate natural remanent magnetization (NRM) variability with age using rock magnetic studies (high-field and k–T experiments, palaeofield intensity determinations by the original Thellier method) together with the good geophysical and geological knowledge of this peculiar segment. NRM intensities range from 1.3 to 25.4 A m^{-1} but do not display any rapid exponential decay with age, as expected. Despite the scatter, they seem to present short-wavelength variations consistent on both flanks of the two lines. Because of the relative uniformity in grain size (i.e. single domain, SD), ulvospinel content (i.e. $x=0.6$) and amount of magnetic minerals in Tammar samples, the observed across-axis NRM intensity variations may be due either to oxidation degree variations or to geomagnetic field intensity changes. Curie temperatures display no increase towards the flanks nor a clear relationship with NRM intensities, suggesting that oxidation degree is not the major process controlling the NRM variations. Half of the collected samples, either fresh or highly altered, provide good-quality palaeointensity determinations. Depending on the alteration degree of samples, two major types of NRM/TRM diagrams are observed. For relatively fresh materials, only one line segment and the major part of NRM is used for field intensity calculations. For moderately or highly altered specimens, two line segments are observed with the first most probably corresponding to thermal demagnetization of the original remanence, and the second to the product resulting from chemical modification (i.e. inversion). Despite the difference in the amount of NRM that can be thermally demagnetized, samples of similar age but of different non-stoichiometric degree give coincident palaeofield strengths. Palaeofield values, from 15 to 62 μT (i.e. VADM from 3.4 to 13.6×10^{22} A m^2), are in good agreement with the global palaeointensity database, and display coherent short-wavelength undulations with age, consistent (assuming a 1-km-wide neo-volcanic zone and steady, symmetrical spreading) with the relative palaeointensity record deduced from sediment core analysis (Guyodo & Valet 1999). Comparison between NRM and field intensity variations with age reveals a remarkable coincidence between both signals, suggesting that the NRM intensities are more sensitive to the field intensity than to the alteration degree. These observations suggest that magnetic particles are titanomaghemites, generated during the initial magma cooling and storing a durable record of the geomagnetic field intensity. The type of remanence is either (1) a chemical remanent magnetization that closely mimics the properties of the initial NRM or (2) a thermoremanent magnetization (the maghemitization precedes the TRM acquisition) or (3) a mixture of both.

Key words: Mid-Atlantic ridge, natural remanent magnetization, palaeointensity, titanomaghemite, titanomagnetite.

1 INTRODUCTION

In addition to providing a robust record of geomagnetic reversals, marine magnetic anomalies exhibit short-wavelength fluctuations, the 'tiny wiggles' (Cande & Kent 1992), superimposed on the main anomalies on both surface and near-bottom magnetic measurements. The youngest 'tiny wiggle', the Central Anomaly Magnetic High (CAMH, Klitgord 1976), is observed at the ridge axis and has been interpreted in terms of spreading processes: more pervasive alteration at fault zones (Klitgord *et al*. 1975; Klitgord 1976; Hussenoeder *et al*. 1996) or geochemical variations of the extrusive basalts and of the magnetic carrier (Prévot & Lecaille 1976) have been proposed to produce alternately high and low magnetized zones. Conversely, the systematic occurrence of the CAMH and of older 'tiny wiggles' has suggested a geomagnetic origin (Cande & Labrecque 1974; Cande & Kent 1992; Gee *et al.* 1996), associated with geomagnetic field intensity fluctuations such as those revealed by archaeomagnetic data (McElhinny & Senanayake 1982).

Natural remanent magnetization (NRM) intensities of submarine oceanic basalts of the Atlantic (Irving *et al.* 1970; Johnson & Atwater 1977) and Pacific (Gee & Kent 1994; Johnson & Tivey 1995) oceans show a rapid decay with age, ascribed to low-temperature oxidation of the titanomagnetite (TM). Very different values of the characteristic time of this decay have been proposed ranging between 20 (Gee & Kent 1994) and 500 kyr (Johnson & Atwater 1977). It should be pointed out that most sample collections are either too sparse or encompass too narrow a section of oceanic crust to resolve the short-wavelength variations recorded by magnetometers.

During cruise Tammar of R/V Nadir and submersible Nautile (May 1996, Gente *et al*. 1997), 11 dives crossed the centre of a highly magmatic ridge segment (Gente *et al*. 1997; Thibaud *et al.* 1998) located between 21°25′ and 22°N on the Mid-Atlantic Ridge (MAR). These dives represent two long cross-sections (hereafter designated Line 1 and Line 2) encompassing the oceanic crust created between 0 and 1.5 Ma. Line 1 (dives 6, 3, 2 and 4) intersects the axial valley at 21°45′N and Line 2 (dives 9, 8, 10, 16, 17, 5 and 7) at 21°40′N (Fig. 1). A deep-sea three-component magnetometer (Ocean Research Institute of the University of Tokyo) installed on the submersible continuously measured the magnetic field along the submersible tracks. Due to the proximity of the magnetic source layer (altitude 1–10 m), near-bottom magnetic measurements

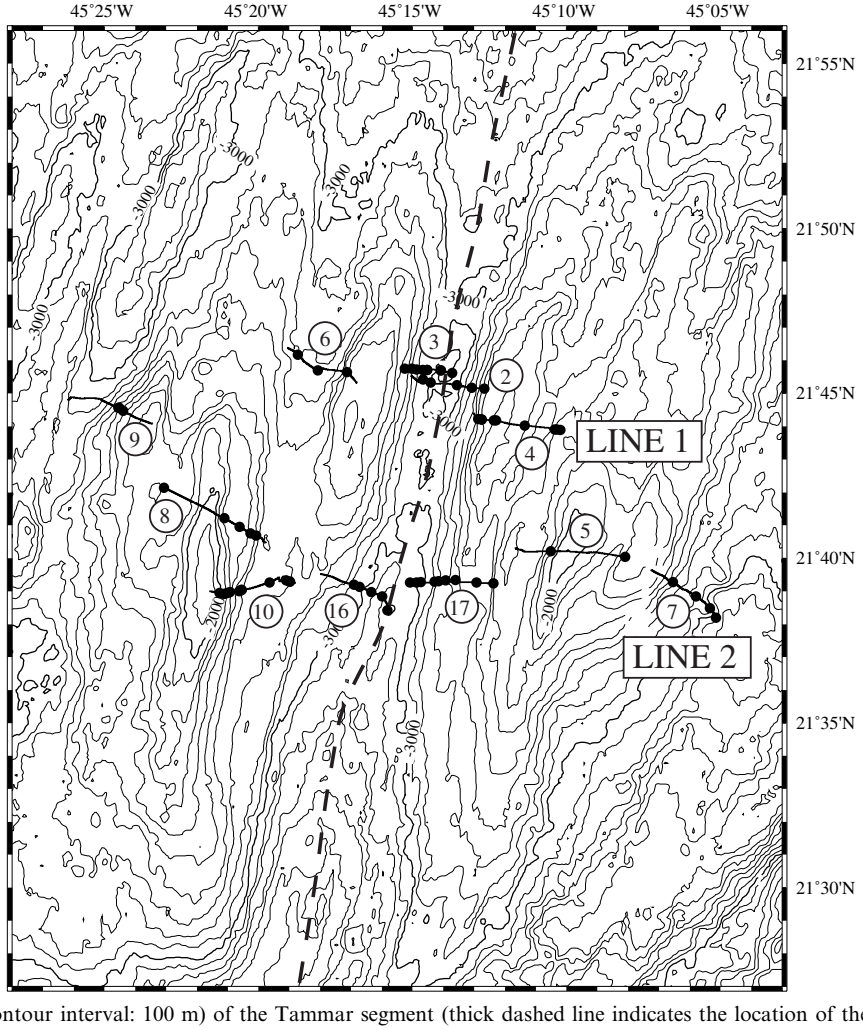

Figure 1. Bathymetry (contour interval: 100 m) of the Tammar segment (thick dashed line indicates the location of the ridge axis). Filled circles indicate the location of the 66 oceanic submarine basalts collected during the dives (thick lines). Line 1 corresponds to the projection of dives 6, 3, 2 and 4 orthogonally to the axis at 21°45'N and Line 2 to dives 9, 8, 10, 16, 17, 5 and 7 projected orthogonally to the axis at 21°40′N.

provide a high-resolution record of short-wavelength variations. The total field intensity of the magnetic data collected along Lines 1 and 2 is presented in Fig. 2(a). Although these data are not corrected for the up-and-down motion of the submersible (i.e. very short-wavelength variations of high amplitude) and latitude effects, they present systematic across-axis short-wavelength (i.e. about 1 km) variations (Honsho *et al.* 1997, 1999). Sea-surface magnetic data also present successive short-wavelength variations; one of these intersects the middle of the axial magnetic anomaly and is interpreted as the CAMH.

In this study, we take advantage of the large number of basaltic rock samples (66) collected at regular intervals along the two cross-sections (Fig. 1) to investigate in detail NRM intensity variations with age from 0 to 1.5 Myr. Determination of the intrinsic magnetic properties of the NRM-bearing particles (i.e. grain size and Curie points) together with detailed knowledge of the morphological, geophysical and geochemical characteristics of this peculiar MAR segment are used to investigate a possible relationship linking the NRM intensity variations with the spreading processes. In addition, geomagnetic field palaeointensities have been determined on these rock samples using the original Thellier method (Thellier & Thellier 1959). Because palaeointensity determination requires material that has not undergone *in situ* alteration, it may seem risky to use samples that have most probably been altered in their early history. However, recent altered submarine basaltic rocks (Grommé *et al.* 1979; Kent & Gee 1996) and basaltic glasses (e.g. Pick & Tauxe 1993) have already provided accurate field intensity determinations, suggesting that either the chemical remanent magnetization (CRM) mimics the properties of the initial thermoremanent magnetization (TRM) (e.g. Grommé *et al.* 1979; Kent & Gee 1996) or the original TRM is durably stored by pristine fine-grained TM (Zhou *et al.* 1999).

2 CROSS-AXIS NRM INTENSITY VARIATIONS AT THE CENTRE OF THE TAMMAR SEGMENT

The NRM intensity was measured on 66 half-specimens, 1 cm long and 2.5 cm in diameter, at the University of Montpellier (France) in a non-magnetic room using a JR5 spinner magnetometer (specified accuracy of 1 per cent). In order to investigate the cross-axis variations of NRM intensity as a function of the distance to the ridge axis, dive tracks and sample locations have been projected on two lines crossing the spreading axis orthogonally at 21°45′N (Line 1) and 21°40′N (Line 2).

The spreading axis can be determined either by the evidence of most recent volcanism through *in situ* observations or as the centre of symmetry of the morphology. However, both methods are not straightforward, as bias may result from the finite width of the neovolcanic zone (NVZ) and possible asymmetrical spreading. In the central part of the Tammar segment, the morphology of abyssal hills is perfectly symmetrical. The most recent volcanoes are 350 m (Line 1) and 230 m (Line 2) away from the morphological centre of symmetry. Because these offsets are in the range of the NVZ width, estimated within 500 and 2000 m for the MAR (Gente *et al.* 1991, 1997), no asymmetrical spreading is considered and the morphological axis is adopted (km 0 in Figs 2, 5, 9a, 11a and b and 12a).

Near-bottom magnetic profiles collected on Line 2 during dives 8 and 5 cross the Brunhes–Matuyama boundary on the western and eastern ridge flanks, respectively (Honsho *et al.* 1999) (Fig. 2a). These determinations provide an estimated half-rate of 12.6 km Myr^{-1} throughout the Brunhes period, used to convert distances from the spreading axis in 'pseudo-ages'. These 'pseudo-ages' are based on the assumption of a steady and symmetrical spreading process. The confidence of the 'pseudo-ages' is investigated using the so-called 'Cassignol technique'. This alternative method to the conventional absolute radiometric K–Ar technique (Gillot & Cornette 1986) compares the isotopic composition of an aliquot of pure atmospheric Ar with the sample Ar. Because the Cassignol technique allows accurate determinations of minor variations of the $^{40}Ar/^{39}Ar$ isotopic ratios between the standard and the unknown, it can be applied to date recent submarine tholeiitic basalts (Vlastelic *et al.* 1998). Four unaltered samples were selected for this geochronological study. Basaltic glasses are avoided as a result of possible excess argon due to rapid quenching. Samples are crushed and sieved to 0.250–0.125 mm size fractions and ultrasonically washed in acetic acid. Phenocrysts and xenocrysts, which may carry excess ^{40}Ar are removed using densities and magnetic separations. K–Ar measurements are performed on the groundmass fractions of each sample: K is analysed by emission spectrophotometry, while Ar is extracted from 1–2 g of sample by radiofrequency heating induction and analysed using a mass spectrometer. Identical ages were obtained for only one sample (103, Line 2, km 5.6 on the western flank), leading to one whole-rock absolute age determination (see Table 1). At this site, the 'pseudo-age' (440 kyr) is similar to the absolute K–Ar age (487 ± 50 kyr), which gives more confidence on the reliability of the 'pseudo-ages' in the area.

The measured NRM intensities range from 1.3 to 25.4 A m^{-1} (see Table 2) with an arithmetic mean value of 10.4 A m^{-1} (i.e. 8.8 A m^{-1} when normalized to the equator). Fig. 2(a) displays NRM intensities variations as a function of the distance from the spreading axis along Lines 1 and 2. Unlike previous studies (Irving 1970; Johnson & Merril 1972, 1973; Marshall & Cox 1972; Johnson & Atwater 1977), no rapid decay of the NRM intensity is observed towards the ridge flanks. Although scattered, NRM intensities seem to present quite consistent short-wavelength (i.e. about 1 km) variations on both flanks of

Table 1. Results of two absolute K–Ar age dating techniques using sample 103 (column 1: percentage of potassium; columns 3 and 4: percentage and amount of radiogenic argon). Age calculations are based on the decay and abundance constants from Steiger & Jäger (1977).

K (wt. %)	Weight molten (g)	$^{40}Ar^*$ (%)	$^{40}Ar^*$ (10^{-13} mol g^{-1})	Age (kyr)	Age mean value (kyr)
0.120 ± 0.001	1.02514	0.304	0.954	458 ± 52	
0.120 ± 0.001	1.11558	0.258	1.075	517 ± 47	487 ± 50

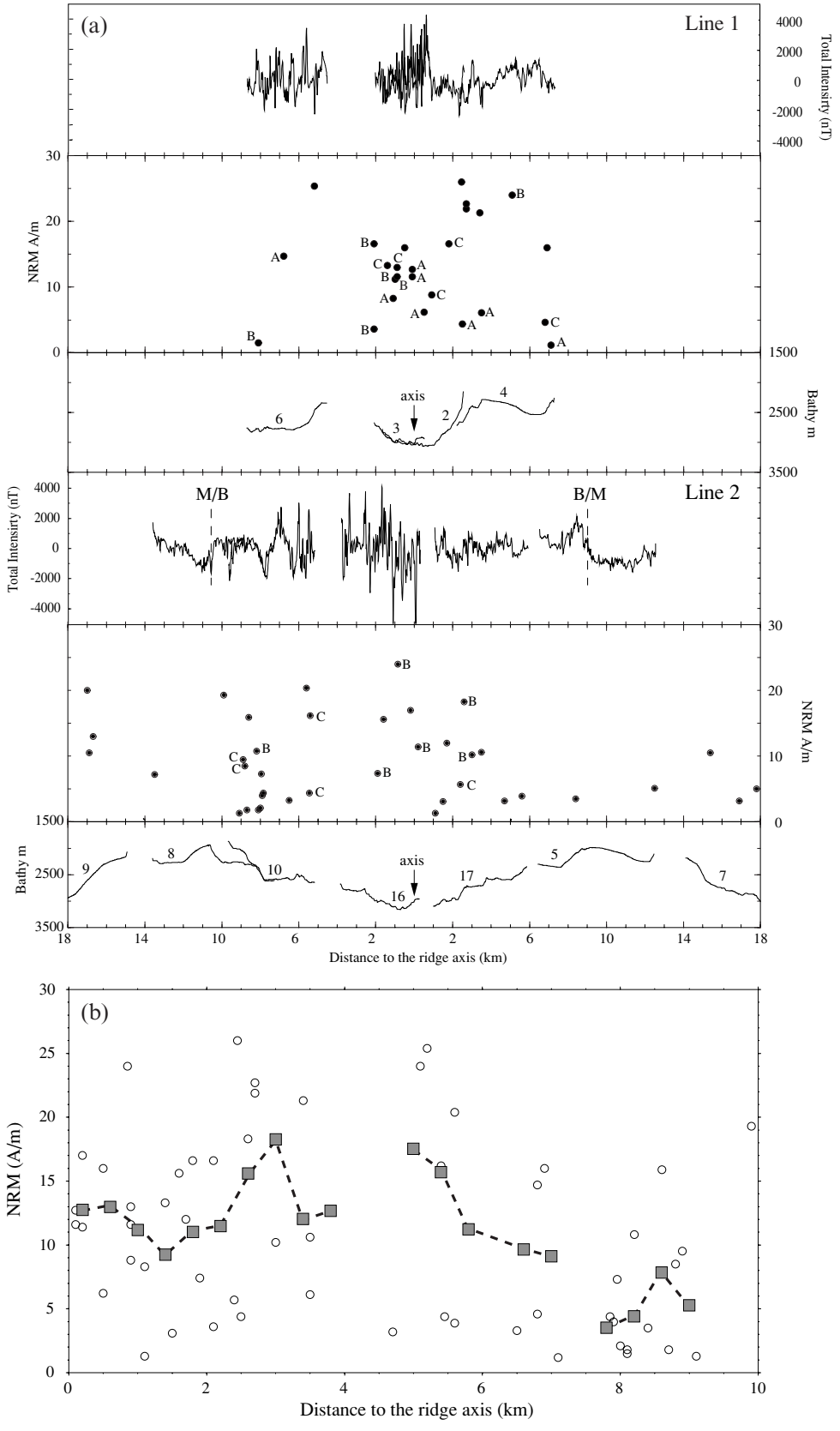

Figure 2. (a) Total intensity of the near-bottom magnetic data. NRM intensities and cross-axis bathymetric profiles as a function of the distance to the ridge axis along Lines 1 (upper three diagrams) and 2 (lower three diagrams). On the NRM diagram, letters denote the distance of the core from the glassy rim (if observed) with A corresponding to distances between 0 and 1 cm, B between 1 and 3 cm and C exceeding 3 cm. (b) NRM intensities of both lines and both flanks reported on the same *x*-axis for distances between km 0 and km 10. Squares denote running averages (width of 0.4 km).

Table 2. Results of magnetic measurements. From left to right (columns 1–20): 1 label of specimen expressed as dive, sample (e.g. 902: dive 9, second sample); 2, 3, 4 sample locations as longitude, latitude and distance from the ridge axis in km ($P_o<0$: western flank, $P>0$: eastern flank); 5 pseudo-age (Myr) estimated using P_o and constant. symmetrical spreading rate; 6 NRM intensity (A m^{-1}); 7 susceptibility corrected for specimen volume (10^{-6} SI); 8 Curie (T_c) and 'pseudo-Curie' temperatures (indicated with star) (see text for explanation); 9 alteration degree; 10, 11, 12 field intensity (μT), uncertainty on the calculation (μT). VADM (10^{22} Am^2); 13–18 high-field experiments with J_{rs}, J_s (10^{-3} A m^2 kg^{-1}); H_{cr}, H_c (mT); ratios J_{rs}/J_s and H_{cr}/H_c; 19, 20 distance (dgr in cm, −1 if glassy margin not observed) and orientation (pgr: pa if parallel, pe if perpendicular) of the core from the glassy rim.

No	Long. °W	Lat. °N	P_o km	Pseudo -age Myr	NRM A m^{-1}	k 10^{-6} SI	T_c and pseudo-T_c*	Alteration degree	F mT	dF mT	VADM 10^{22} A m^2	J_{rs} 10^{-3} A m^2 kg^{-1}	J_s 10^{-3} A m^2 kg^{-1}	H_{cr} mT	H_c mT	J_{rs}/J_s	H_{cr}/H_c	dgr cm	pgr
902	45.4093	21.7428	−17	−1.35	20	2520						267	394	34.3	34.5	0.68	0.99	3	pa
903	45.4087	21.7427	−16.9	−1.34	10.5	4620												3	pa
905	45.4066	21.7412	−16.7	−1.33	13	2040												0.5	pa
806	45.3845	21.7023	−13.5	−1.07	7.2	1020	290*	0.5	30.5	0.6	6.64	102	132	10.9	9.6	0.77	1.14	2	pa
805	45.3518	21.687	−9.9	−0.79	19.3	2440												−1	
114	45.3544	21.649	−9.1	−0.72	1.3	640			28	0.4	6.1							−1	
803	45.3435	21.6826	−8.9	−0.71	9.5	6020												3	pa
113	45.3518	21.6486	−8.8	−0.7	8.5	2840												3	pa
112	45.3502	21.649	−8.7	−0.69	1.8	14440												−1	
109	45.3488	21.6496	−8.6	−0.68	15.9	6220												−1	
802	45.3376	21.6793	−8.2	−0.65	10.8	2540	240*	0.35	22.6	0.9	4.92	107	144	69.3	62.7	0.74	1.11	2	pa
108	45.3439	21.65	−8.1	−0.64	1.8	800	255*	0.4	16.3	0.4	3.55	101	138	79.4	67.9	0.73	1.17	−1	
107	45.3432	21.6502	−8	−0.63	2.1	12580												−1	
106	45.3425	21.6506	−7.95	−0.63	7.3	3140												−1	
105	45.3423	21.6506	−7.9	−0.63	4	17660												−1	
801	45.3347	21.6782	−7.85	−0.62	4.4	19840	180	0.1	34.1	1.2	7.43	107	796	14	5.1	0.13	2.75	−1	
104	45.3272	21.6544	−6.5	−0.52	3.3	800	265*	0.4	30.4	0.5	6.62	73	103	79.6	66.9	0.71	1.19	−1	
103	45.3184	21.6554	−5.6	−0.44	20.4	2700			42.7	1.2	9.3	214	302	37.8	38.6	0.71	0.98	−1	
102	45.3164	21.6548	−5.45	−0.43	4.4	800	380*	0.7	39.9	1.7	8.69	60.5	83	114	92.7	0.73	1.23	3.5	pa
101	45.3162	21.6547	−5.4	−0.43	16.2	3080	215	0.2	42	0.3	9.15	233	408	23.6	21.6	0.57	1.09	3	pa
168	45.2817	21.6532	−1.9	−0.15	7.4	3000	160	0.05	34.8	1.3	7.58	132	231	25.2	20.3	0.57	1.24	2	pa
167	45.2785	21.6521	−1.6	−0.13	15.6	3320	200	0.15	41.1	0.9	8.95	182	335	24.1	20	0.54	1.21	−1	
166	45.2722	21.6496	−0.85	−0.07	24	8280			37.7	0.4	8.21							1	pa
164	45.2664	21.6474	−0.2	−0.02	17	10500												−1	
161	45.2635	21.6402	0.2	0.02	11.4	5340	195	0.15	51.4	2	11.2	155	324	20.7	14.7	0.48	1.41	2	pa
711	45.2512	21.6543	1.1	0.09	1.3	720			15	0.4	3.27							−1	
712	45.2477	21.6543	1.5	0.12	3.1	940			25.2	0.8	5.49							0.3	pa
713	45.2455	21.6545	1.7	0.13	12	7200			22.7	1	4.95	216	420	17.2	13.6	0.51	1.26	−1	
714	45.2382	21.6549	2.4	0.19	5.7	3500	310*	0.5	24.2	1	5.27	166	336	34.1	27.5	0.49	1.24	2.5	pa
715	45.236	21.6551	2.6	0.21	18.3	3360	250*	0.35	31.8	0.6	6.93	229	354	34.4	31.6	0.65	1.09	1	pa
716	45.2321	21.6555	3	0.24	10.2	8880												2	pa
717	45.2279	21.6449	3.5	0.28	10.6	8620												−1	
720	45.2154	21.6544	4.7	0.37	3.2	2640												−1	
721	45.2064	21.654	5.6	0.44	3.9	7460												−1	
502	45.1753	21.6702	8.4	0.67	3.5	11920												−1	
506	45.135	21.6673	12.5	0.99	5.1	1300						117	165	45.3	38.8	0.71	1.17	−1	
705	45.1092	21.6546	15.4	1.22	10.5	2260						208	308	49.7	45.2	0.68	1.1	−1	
703	45.0967	21.6473	16.9	1.34	3.2	880			15.5	0.5	3.38	117	154	75.8	67.8	0.76	1.12	−1	
702	45.0891	21.6414	17.8	1.41	5	1520			18.8	0.3	4.1	146	199	91.4	79.4	0.73	1.15	−1	
701	45.0858	21.6365	18.2	1.44	1.7	3380												−1	

Table 2. (*Continued.*)

No	Long. °W	Lat. °N	P_o km	Pseudo -age Myr	NRM A m^{-1}	k 10^{-6} SI	T_c and pseudo-T_c^*	Alteration degree	F mT	dF mT	VADM 10^{22} A m^2	J_{rs} 10^{-3} A m^2 kg^{-1}	J_s 10^{-3} A m^2 kg^{-1}	H_{cr} mT	H_c mT	J_{rs}/J_s	H_{cr}/H_c	dgr cm	pgr
601	45.3119	21.7697	−8.1	−0.64	1.5	560			18.3	0.5	3.99							1.5	pa
602	45.3012	21.7618	−6.8	−0.54	14.7	1080			32.3	1	7.04							0.1	pa
606	45.2855	21.7609	−5.2	−0.41	25.4	5420			62.3	0.6	13.6	149	297	43	31.4	0.5	1.37	−1	
313	45.2503	21.7625	−2.1	−0.17	3.6	1060			23.2	0.5	5.05							1	pe
312	45.2542	21.7625	−2.1	−0.17	16.6	3340	230	0.3	27.1	0.5	5.9	194	278	39.1	38	0.7	1.03	2	pa
309	45.2478	21.7621	−1.4	−0.11	13.3	7320						173	419	21.3	15.2	0.41	1.4	7	pa
308	45.2445	21.762	−1.1	−0.09	8.3	2440			23	0.9	5.01	111	148	79	73.2	0.75	1.08	0.1	pa
201	45.2443	21.757	−1	−0.08	11.2	5140												1.5	pa
306	45.2422	21.7619	−0.9	−0.07	13	5900						178	371	20.5	15.4	0.48	1.33	7	pa
305	45.2422	21.7619	−0.9	−0.07	11.6	3120			23.9	0.3	5.21							2	pa
202	45.2402	21.7555	−0.5	−0.04	16	13800						183	617	14.8	8.45	0.3	1.75	−1	
304	45.2349	21.7617	−0.1	−0.01	12.7	2060			48.2	0.6	10.5	92	151	50.7	39.4	0.61	1.29	0.5	pa
303	45.2349	21.7617	−0.1	−0.01	11.6	2080			47.9	1.1	10.4							0.3	pa
301	45.2287	21.7603	0.5	0.04	6.2	960			38.1	0.4	8.3							0.5	pa
204	45.2261	21.7542	0.9	0.07	8.8	3740						138	250	25.7	21	0.55	1.22	2.5	pa
207	45.2181	21.7529	1.8	0.14	16.6	6720			32.2	0.3	7.01	166	316	25.2	20	0.53	1.26	8	pa
208	45.2113	21.7524	2.45	0.19	26	7500												−1	
401	45.2146	21.7371	2.5	0.2	4.4	880	310*	0.5	31.3	0.8	6.82	46.5	66	156	122	0.7	1.28	0.5	pa
402	45.2127	21.7369	2.7	0.21	21.9	13760	130	0				201	612	12.8	8.5	0.33	1.51	−1	
403	45.2126	21.7369	2.7	0.21	22.7	9900						186	510	14.6	10.5	0.36	1.39	−1	
405	45.206	21.7364	3.4	0.27	21.3	7880												−1	
406	45.2048	21.7365	3.5	0.28	6.1	1000			35.5	0.7	7.73	138	184	60.1	59.2	0.75	1.02	0.5	pa
407	45.1893	21.7337	5.1	0.4	24	4480												2	pa
409	45.1731	21.7318	6.8	0.54	4.6	960												3.5	pa
410	45.172	21.7319	6.9	0.55	16	1780												−1	
411	45.1701	21.7316	7.1	0.56	1.2	360			29.3	0.6	6.38							0.5	pa

the two lines, especially for the best sampled area between the spreading axis (km 0) and km 3. To investigate this trend further, the NRM intensities of both lines and both flanks are reported together as a function of the distance from the spreading axis, and a mean calculated each 0.4 km (Fig. 2b). Mean NRM intensities (squares on Fig. 2b) reach 13 A m^{-1} at the axis, decrease to 9 A m^{-1} at km 1 (i.e. 80 kyr) and increase to about 20 A m^{-1} at km 3 (i.e. 240 kyr). Data are sparser beyond km 3. NRM intensities exceed 15 A m^{-1} at km 5 (i.e. 400 kyr) and decrease to about 10 A m^{-1} at km 7 (i.e. 560 kyr).

3 FACTORS LEADING TO NRM INTENSITY VARIABILITY

Titanomagnetite (TM) is the NRM carrier in submarine oceanic basalts (e.g. Petersen *et al.* 1979). NRM intensities depend on grain size, magnetic chemical composition, quantity of TM and geomagnetic field intensity at the time of magnetization acquisition. One or a combination of several of these parameters is likely to generate the observed NRM intensity variations. We investigate the effect of each parameter on the Tammar samples in order to discriminate the dominant effect accounting for the observed NRM intensity variations.

3.1 Grain size effect

Electron microscope observations of submarine basalts from the MAR has revealed abundant TM grains finer than 0.1 μm in diameter (Bleil & Smith 1979). These very fine-grained particles result from the rapid quenching of the basalts. However, grain size displays significant variations inside a pillow lava as a function of cooling rate and hence of the distance from the chilled margin (Marshall & Cox 1971; Ryall & Ade-Hall 1975; Kent & Gee 1996; Zhou *et al.* 1997). It is worth noting that the glassy rim is not observed on all pillow lava samples collected during the Tammar cruise. When the glass rim is preserved and where possible, specimens were cored within several millimetres to 4 cm of the chilled margin (see Table 2).

The most pertinent means for diagnosing the domain structure are the ratio of the remanent saturation magnetization to the saturation magnetization (J_{rs}/J_s) and of the remanent coercive force to the coercive force (H_{cr}/H_c). 32 samples have been selected for high-field magnetic experiments. Hysteresis loops were realized using an automatic mini-translation inductometer placed within the gap of an electromagnet providing fields as high as 1 T (laboratory-made instrument, Saint-Maur laboratory, Paris). The grain size dependence of NRM intensities can be confidently estimated because halves of the same cores were used for NRM and high-field magnetic measurements. Fig. 3 illustrates four examples of magnetic curves obtained during the high-field experiments. Corrected for paramagnetism, J_{rs}/J_s and H_{cr}/H_c ratios of all but seven analysed samples range from 0.48 to 0.77 and from 1.02 to 1.37, respectively (see Table 2). However, some samples (e.g. Figs 3c and d) were not fully saturated in the maximum applied field (0.7 T). H_{cr}/H_c ratios of 1 are attributed to samples 103 and 902, for which the observed ratios less than unity (i.e. 0.98 and 0.99, respectively) are considered an artefact due to the limit of resolution on H_{cr} (calculations based on only two points).

Considering the limits given for TM (Day *et al.* 1977), these ratios indicate grains with a single-domain (SD) assemblage. Specimens 202, 309, 402, 403 and 801 show lower J_{rs}/J_s (from 0.13 to 0.41) and higher H_{cr}/H_c (from 1.39 to 2.75) ratios, suggesting coarser grains in a pseudo-single-domain (PSD)

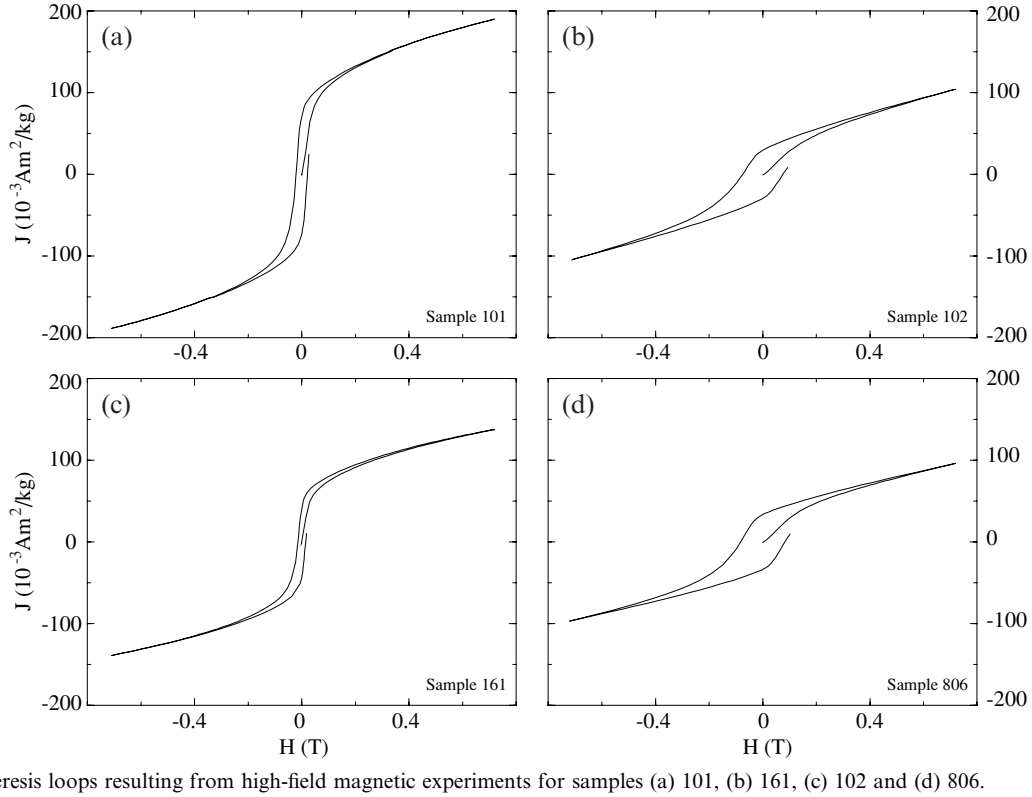

Figure 3. Hysteresis loops resulting from high-field magnetic experiments for samples (a) 101, (b) 161, (c) 102 and (d) 806.

assemblage. No significant discrepancy is observed between the NRM intensities of the finer and coarser grains (see Table 2).

Although hysteresis loop ratios indicate a rather uniform grain size assemblage, NRM intensities and their scatter depend on the distance from the glassy margin (Fig. 4). Three zones can be defined inside a pillow lava. Zone A corresponds to the outer part of the pillow (less than 1 cm from the glassy rim) and displays relatively low and grouped NRM values ranging from 1 to 15 A m^{-1}. Zone B, between 1 and 3 cm from the margin, is associated with greater and more scattered NRM values from 4 to 25 A m^{-1}. Zone C, the inner part of the pillow, shows somewhat lower NRM intensities ranging from 4 to 20 A m^{-1}. These observations seem consistent with the peak in NRM intensity observed near the glassy rim (i.e. between 1 and 3 cm) of individual pillow basalts from the Juan de Fuca axis and ascribed to very fine-grained TM either preferentially oxidized (Kent & Gee 1996) or with a peculiar chemical composition (Zhou *et al.* 1997).

The locations of the cores are shown in Fig. 2(a) (A: less than 1 cm of the glassy rim; B: between 1 and 3 cm; C: more than 3 cm) for estimating grain size effect on the across-axis NRM intensity variations. The highest NRM values are not systematically associated with the finest-grained particles (i.e. B), while specimens cored either in the outer part of the pillow (i.e. A) or in its inner part (i.e. C) do not systematically correspond to the lowest NRM intensities. These observations, together with the relative consistency of NRM intensity variations on both flanks and both lines, suggest that across-axis NRM variations are not primarily related to grain size effects resulting from a sampling bias.

3.2 Magnetic carrier content

Extrusive basalts are tholeiites of rather uniform composition and may contain as much as 5 per cent TM, although more commonly 1–2 per cent. Variations in the content of magnetic minerals may result in important variations of NRM intensities. An indirect means for estimating the amount of magnetic carrier in the submarine oceanic basalts is the contents of FeO and TiO_2 in the basaltic glass. Magnetic telechemistry hypothesis (Vogt & Johnson 1973) suggests the association of high-amplitude magnetic anomalies with FeO–TiO_2-enriched lavas as a result of a relationship linking the Fe–Ti enrichment with enhanced NRM values (Gee & Kent 1998).

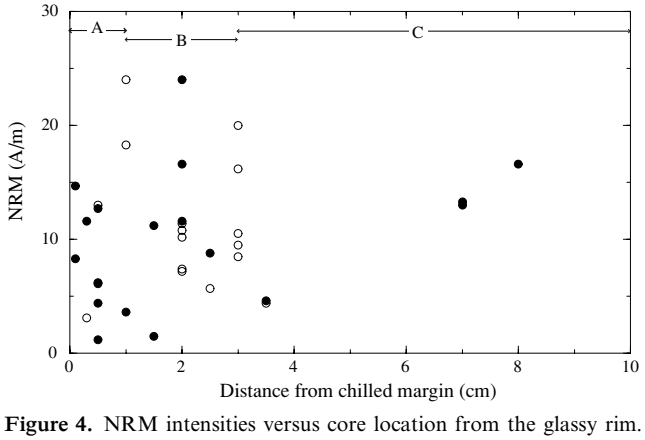

Figure 4. NRM intensities versus core location from the glassy rim. Filled circles correspond to samples of Line 1 and open circles to those of Line 2.

Axial morphology, gravity anomaly (Thibaud *et al.* 1998) and *in situ* evidence of recent lava lakes at the segment centre (Gente *et al.* 1997) suggest that the Tammar segment is a 'hotter segment' (Thibaud *et al.* 1998) associated with robust magmatic activity. As a consequence, the relatively high magma supply rate may result in open systems in which magma compositions do not reach advanced fractionation degree (Sinton *et al.* 1983). The absence of significant modification by low-pressure fractionation prior to eruption is confirmed by the rather uniform and low FeO and TiO_2 contents (from 8.5 to 10 per cent and from 1.15 to 1.70 per cent, respectively) (Fig. 5) analysed on whole-rock powders (G. Ceuleneer, personal communication, 1997). Although homogenous, both FeO and TiO_2 contents display slight monotonic increases away from the axis but at a wavelength inconsistent with that of the NRM intensity variations.

3.3 Chemical composition of the magnetic carrier: estimation of x and z

The composition parameter, x, defines the ulvospinel content in the TM structure: $Fe_{3-x}Ti_x0_4$. For TM of oceanic basalts, x is commonly 0.6 at the time of crystallization (Smith 1984) but may vary between 0.5 and 0.65 (Ryall & Ade-Hall 1975; Grommé & Mankinen 1976).

As the magnetization of TM depends on x, alternating high and low NRM intensities may reflect high and low Ti-contents, respectively, in the TM structure. An unequivocal method for estimating the chemical composition of natural stoichiometric and non-stoichiometric TM (i.e. respectively unaltered TM and titanomaghemite) is to determine two of the following parameters: Ti/Fe ratio, unit cell edge and Curie temperature. Previous studies have shown that direct measurements of chemical composition on very fine-grained particles are difficult with a microprobe (Grommé *et al.* 1979; Kent & Gee 1996; Horen & Fleutelot 1998) and require high-resolution electron microscopy studies (e.g. Zhou *et al.* 1997). However, such

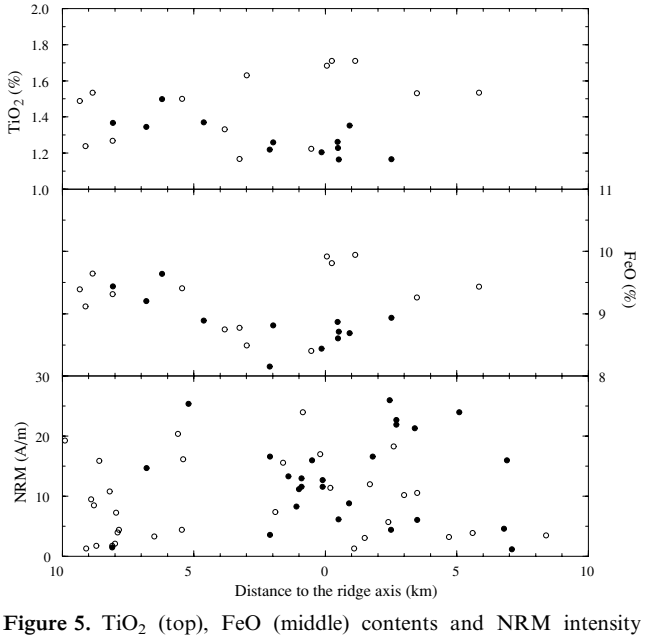

Figure 5. TiO_2 (top), FeO (middle) contents and NRM intensity variation (bottom) as functions of the distance to the axis. Open circles correspond to samples of Line 2 and filled circles to those of Line 1.

measurements on a given grain may not be representative of the bulk specimen, while large variations in the x-content are expected between adjacent grains (Zhou *et al.* 1997). Conversely, Curie temperature (T_c) is determined on the whole rock and accounts for the bulk specimen.

The x-content of the NRM magnetic carriers will be roughly estimated through the use of T_c only. With respect to the high-field experiments, which indicate SD assemblage (see Section 3.1), T_c is considered as representative of the finest-grained magnetic carriers (that is, the grains that carry the major part of the NRM) and not of the MD population, as suggested by Kent & Gee (1994, 1996). T_c is not only x-dependent. Minor elements, such as Al and Mg substituted for Fe in the TM structure and the oxidation parameter, z, which reflects the fraction of Fe^{2+} in the stoichiometric composition transformed to Fe^{3+} (Readman & O'Reilly 1972), are factors affecting T_c (Smith 1984). An approximate method to estimate the global x-content of the sample from T_c is to attribute the lowest observed T_c to a stoichiometric (i.e. unaltered) and pure (i.e. non-substituted) TM (e.g. Ryall & Ade-Hall 1975; Grommé & Mankinen 1976).

3.3.1 *Curie temperature determination*

T_c can be estimated by considering either the saturation magnetization, J_s, or the weak-field initial susceptibility, k, as a function of the temperature (T). Low-field susceptibility measurements were performed on 15 samples by heating powdered samples (about 500 mg) up to 350 or 600 °C in argon atmosphere using a Kappa-Bridge susceptibility meter associated with a CS3 furnace (Ecole Normale Supérieure, Paris, France). Heating and cooling cycles were carried out at a rate of 6° min^{-1} in order to minimize the temperature lag between the sample and the thermocouple. Two types of k–T curves, hereafter designed types A and B, are observed (Fig. 6).

Half of the analysed samples show a heating curve (type A) with a single pronounced susceptibility peak before falling to near zero (Figs 6a and b). This peak is ascribed to the Hopkinson peak effect and used to determine T_c. However, as pointed out by Prévot *et al.* (1983), T_c in natural bulk rocks is broadly distributed around a mean value. A minimum T_c is estimated using the inflection point of the k–T or J_s–T curves (method of Chevallier & Pierre 1932), while the intersection between the appropriate base line and the tangent to the inflection point (method of Grommé *et al.* 1979) leads to an estimate of the maximum value of T_c. These two methods can lead to T_c estimations that differ by several tens of degrees (Moskowitz 1981). The method of Grommé *et al.* (1979) has been used, yielding T_c between 130 and 230 °C. Despite an increase in k, the cooling curve closely resembles the heating curve. Such an increase has previously been ascribed to atomic reordering in the crystalline structure without magneto-mineralogical changes (Bina 1990). We therefore consider samples of group A as associated with 'pseudo-reversible' cooling curves (i.e. without mineralogical modifications during heating).

Contrary to this quite simple thermomagnetic behaviour, samples of group B exhibit complex k–T curves showing several susceptibility peaks suggesting the presence of several magnetic phases (Figs 6c and d). Because of the difficulty in estimating the appropriate baseline, the graphical determination of T_c characterizing these magnetic phases is not straightforward. For temperatures above 350 °C, two magnetic phases are recognized, with T_c around 500 °C and 580 °C. Between the susceptibility peak observed at low temperature and 350 °C, the decrease of k with T is either regular, down to an inflection point around 330–340 °C (Fig. 6c), or more complex, with two inflection points, at about 250 °C and between 320 and 340 °C (Fig. 6d). The cooling curve shows only one wide susceptibility peak that does not correspond to those observed on the heating curve. Samples of group B are therefore characterized

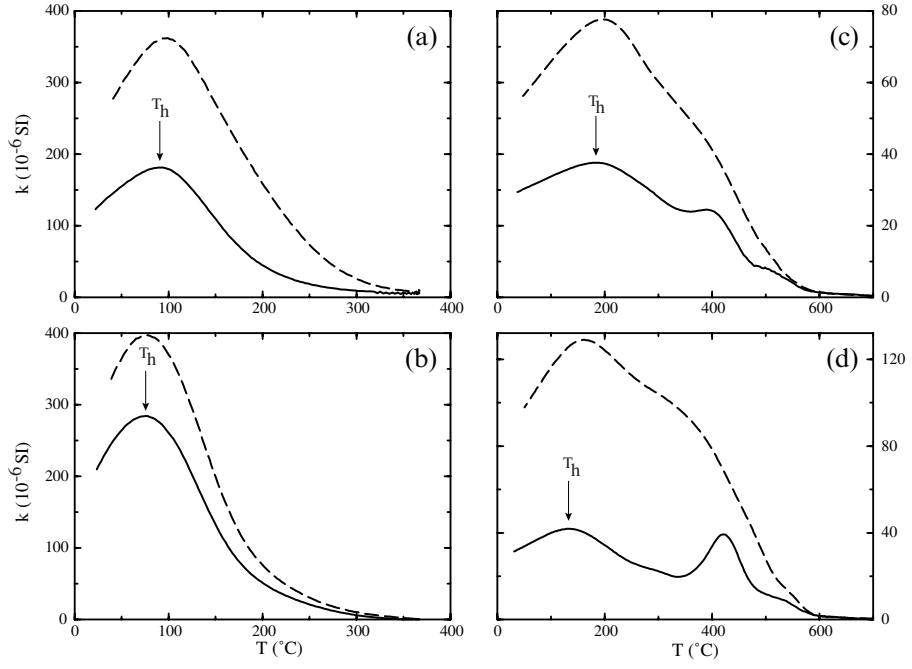

Figure 6. Variations of the low-field susceptibility (not corrected for specimen volume or mass) during one heating (thick line)–cooling (dashed line) cycle for samples of group A (a 101, b 161) and group B (c 102, d 806). See Fig. 3 for corresponding high-field experiments. T_h refers to the temperature corresponding to the Hopkinson peak (see text for explanation).

by irreversible magnetic curves. A signature of the titanomaghemite is its irreversible thermomagnetic curve with unmixing and inversion occurring between 300 and 400 °C (Ozima & Larson 1970; Readman & O'Reilly 1972; O'Reilly 1984). Inversion occurs as a result of the open structure of the titanomaghemites, which collapses towards a more stable configuration at moderate temperatures. O'Reilly (1984) pointed out the difficulty in interpreting the experimental results of inversion because the end product consists of a complicated mixture of magnetic and non-magnetic phases. He gave a 'simplified and possible inversion sequence' including a titanomagnetite/ilmenite intergrowth. We consider that the magnetic phases observed above 250 °C on the k–T heating curves of group B did not exist prior to laboratory heating. The 'low-temperature' original magnetic phase is most probably a titanomaghemite that inverts to a multiphase mixture including a Ti-poor spinel near magnetite (T_c 580 °C) and possibly a titanohaematite with $y=0.2$ (T_c 500 °C) and a TM40 (T_c 350–400 °C). As a result of the inversion, the first observed inflection point (i.e. between 250 and 340 °C) does not correspond to the true T_c of the original magnetic phase but to a dissociation temperature range. This wide range of inversion temperatures may reflect differences in alteration degree, grain size and impurities in the TM structure (O'Reilly 1984).

Interpreting the thermal stability of the sample in terms of alteration degree suggests that magnetic carriers of group A are either fresh or moderately altered TM with reasonably reversible k–T curves, while those of group B are more altered TM that invert before reaching their T_c. Samples of group A present a clear correlation ($R=0.91$) between the temperature of the Hopkinson peak, T_h, and the estimated T_c (Fig. 7), suggesting that T_h characterizes the mineral species as T_c does. For samples of group B, the first magnetic susceptibility high observed on the heating curve corresponds to temperature ranging between 110 and 186 °C, hence below the estimated temperature range of the titanomaghemite inversion. This suggests that only the original magnetic phase is present at this low temperature and that the first susceptibility peak can be ascribed to the Hopkinson effect and used to determine T_c. We consider therefore that (1) T_h can be used to characterize the magnetic phase as T_c is, (2) all analysed samples are characterized by TM whose composition is z-dependent, and (3) for the samples of group B, inversion has not already occurred at T_h. These assumptions allow us to define a 'pseudo-T_c' for the samples of group B, by using T_h and the linear relation linking T_h and T_c for samples of group A. The resulting 'pseudo-T_c' of the initial titanomaghemites range between 240 and 380 °C (see Table 2).

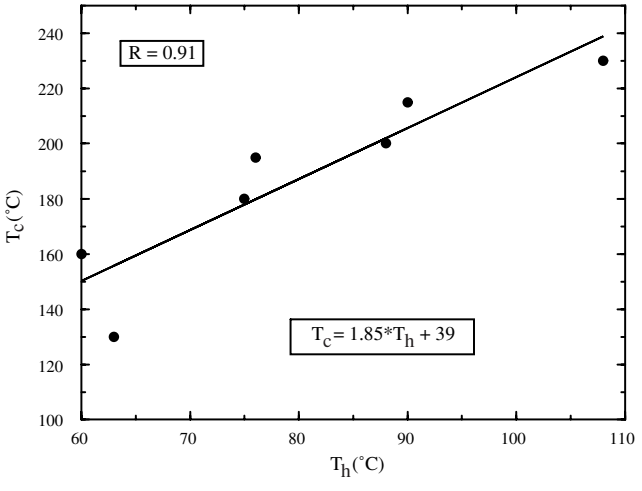

Figure 7. Temperature of the Hopkinson peak versus Curie temperature estimated for samples of group A and result of the linear regression that is used for determining a 'pseudo-Curie' temperature for samples of group B.

3.3.2 *Ulvospinel content estimation*

The lowest T_c among specimens of group A is 130 °C (specimen 402 at km 2.7). From synthetic data of Akimoto *et al.* (1957) and Ozima & Larson (1970), Grommé *et al.* (1979) have computed a least-squares regression linking T_c and x. Using this equation and a T_c of 130 °C leads to a stoichiometric pure TM with $x=0.6$. This estimated ulvospinel content in the TM structure is in agreement with the TM composition commonly found in oceanic basalt (Smith 1984). Considering no substitution by Al and Mg cations in the TM structure leads us to ascribe variations of T_c to either x or z variations. A means of discriminating is the relationship linking initial magnetic susceptibility, k, with T_c. For SD grains, k tends to increase with T_c if the latter varies as a consequence of Ti-content in the crystalline structure. Conversely, if T_c variation is primarily related to z variation, k tends to decrease with T_c for z ranging between 0 and 0.7, and tends to increase with T_c for higher z (Day *et al.* 1977; Prévot *et al.* 1981; Smith 1984; Smith 1987). Fig. 8 displays log(k) as a function of T_c of group A (black circles) and 'pseudo-T_c' of group B (grey circles). Despite the scatter, a negative correlation is unambiguously observed between log(k) and T_c ($R=0.60$). Therefore, T_c variability may principally result from z variability (with z remaining less than 0.7). Previous studies have suggested that Ti-content in the TM structure is dependent on basalt geochemistry and

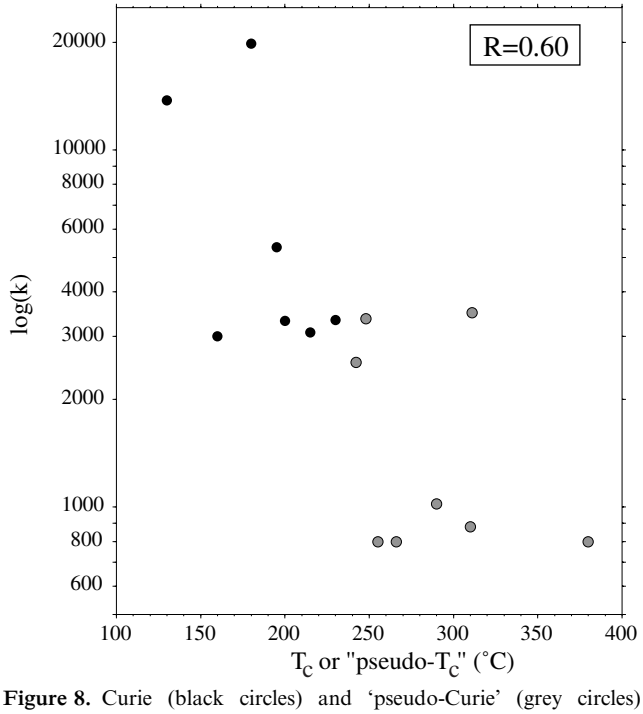

Figure 8. Curie (black circles) and 'pseudo-Curie' (grey circles) temperatures versus initial susceptibilities.

particularly on FeO and TiO_2 glass content (Perfit & Fornari 1983). The rather uniform geochemical composition of the erupted lavas (see Section 3.2) is consistent with the conclusion of a uniform ulvospinel content. These observations preclude a geochemical origin for the observed NRM intensity variations.

3.3.3 Low-temperature alteration

The observed T_c variability for samples of group A (ranging from 130 to 230 °C) corresponds to non-stoichiometric and non-substituted titanomagnetite having z between 0 and 0.25 (O'Reilly 1984). As mentioned above, samples of group B are more altered than those of group A. The 'pseudo-T_c' results in 'pseudo-z' ranging between 0.35 and 0.7.

Fig. 9(a) displays T_c of group A and 'pseudo-T_c' of group B as a function of the distance to the ridge axis. No significant trend is observed with distance, and therefore with age. At km 0.2, a T_c of 195 °C is observed (specimen 161), while at km 2.5 T_c ranges from 130 to 310 °C. Contrary to the observations of Johnson & Hall (1978) using samples from the Nazca plate, NRM intensities of the Tammar samples only display a poor relationship with T_c ($R=0.48$) (Fig. 9b). For group A (black circles in Fig. 9b), NRM intensities are linked to T_c by a positive trend, the highest T_c (i.e. 230 °C corresponding to $z=0.25$) being associated with high NRM values (i.e. 17 A m^{-1}). NRM intensities of group B are scattered, ranging between 1.8 and 18.3 A m^{-1}, quite similar to samples of group A. Therefore, although the Tammar submarine basalts have undergone a significant alteration, the alternation of low and high NRM intensities does not seem to reflect a more or less pronounced alteration degree.

3.4 Field intensity

For a given ferromagnetic material, the intensity of the TRM is proportional to the intensity of the magnetic field at the time of magnetization acquisition. This property is used to determine the absolute intensity of the geomagnetic field through geological time. Practically, samples are heated and then cooled in a known field, hence acquiring a laboratory TRM that is compared to the NRM. These methods therefore assume the NRM to be original TRM unaltered by geological processes. Also, the constant of proportionality has to remain unchanged by the experimental procedure. This last point is a considerable limitation of the palaeointensity determination methods, and stepwise techniques (e.g. Thellier & Thellier 1959) have been proposed to detect changes and estimate the palaeointensity before chemical changes occur. However, the material should satisfy the laws of addition and independence (that is, similarity of the blocking and unblocking temperatures) of partial TRMs acquired in non-overlapping temperature intervals. These criteria were shown to be fulfilled by non-interacting SD grains (Néel 1949; Thellier & Thellier 1959) and also by PSD grains but not by multidomain grains (Shcherbakov *et al.* 1993). The grain size is not a limitation to obtaining reliable palaeointensity determinations from submarine oceanic basalts because their rapid quenching leads to an SD assemblage, as indicated by J_{rs}/J_s and H_{cr}/H_c ratios for most of the Tammar samples (see Table 2 and Section 3.1).

The capacity of the samples to acquire a viscous remanent magnetization (VRM) was estimated prior to palaeointensity analysis. The remanent magnetization was first measured after a 2 week storage with the ambient field applied along the cylindrical (i.e. z-) axis of the specimens, and again after another 2 week period in a field-free space. It is worth noting that in the case of the Tammar samples, the z-axis has no geological significance as the samples were not oriented *in situ.* All but five specimens display very low magnetic viscosity with viscosity index (Thellier & Thellier 1944) less than 5 per cent.

3.4.1 Experimental procedure

Palaeointensity experiments were carried out on the 66 half-specimens used for NRM intensity measurements. The experimental procedure chosen here was the original Thellier method (Thellier & Thellier 1959), which requires a progressive stepwise double heating of the specimens, with a laboratory field (50 μT in our case) applied along the z-axes of the cores in opposite directions during each of the paired heatings. As blocking and unblocking temperatures for SD assemblages are identical, the remanent magnetization intensity measured at a given temperature step after the first heating–cooling cycle is the vectorial sum of the NRM remaining after heating at T (NRM_T) and the TRM acquired from T to room temperature (TRM_T). Conversely, the remanence measured after the second heating–cooling cycle is the vectorial difference between them.

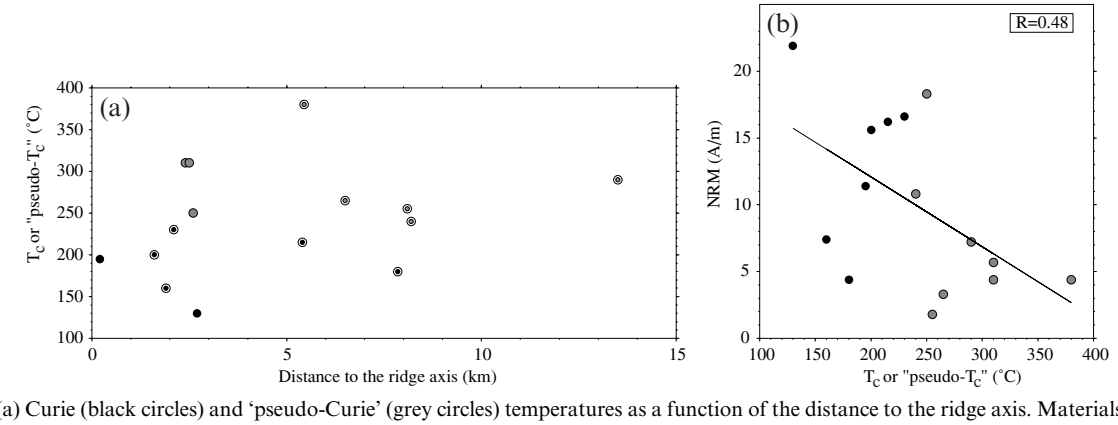

Figure 9. (a) Curie (black circles) and 'pseudo-Curie' (grey circles) temperatures as a function of the distance to the ridge axis. Materials collected on both flanks are reported on the same x-axis: samples of Line 1 are denoted by filled circles and small filled circles surrounded with open circles correspond to samples of Line 2. (b) NRM intensities as a function of Curie (black circles) and 'pseudo-Curie' (grey circles) temperatures.

All experiments were carried out in a 10^{-2} Pa vacuum leading to an increase in the length of experiment time (8–12 hr was necessary for a complete heating–cooling cycle) but preventing, as much as possible, oxidation processes.

In order to detect chemical changes during the course of the experiments, sliding pTRM checks (Prévot *et al*. 1985) were regularly performed with an additional heating–cooling cycle at a temperature lower than the temperature of the last cycle (see NRM–TRM plots, Fig. 10 left). The temperature reached by the specimens was precisely monitored by three thermocouples located within fictitious samples evenly spaced along the sample holder. Sample location in the furnace is identical at

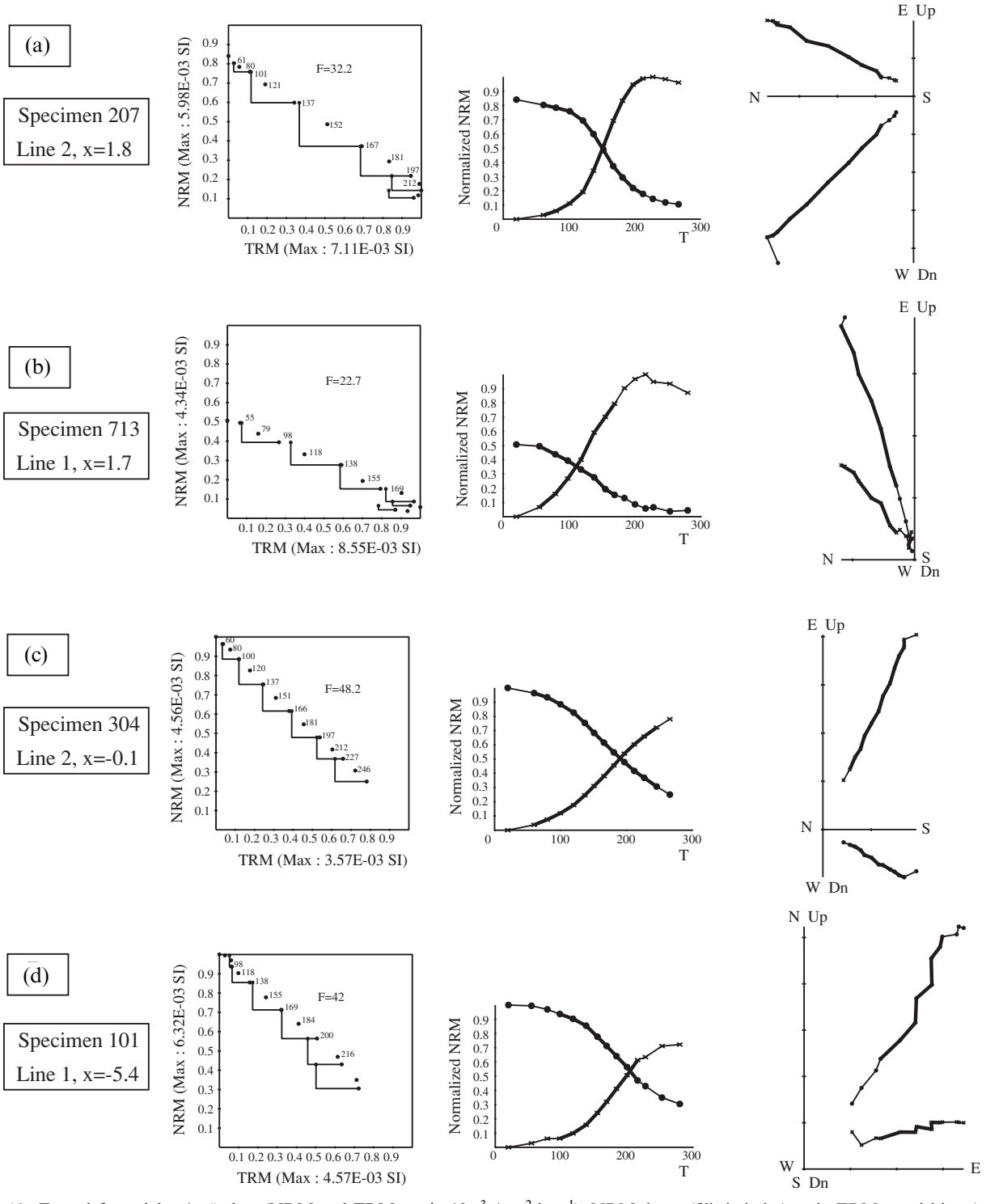

Figure 10. From left to right: Araï plots (NRM and TRM are in 10^{-3} A m^2 kg^{-1}); NRM decay (filled circles) and pTRM acquisition (crosses) plotted as a function of temperature; and vector-endpoint diagrams for samples (a) 207, (b) 713, (c) 304, (d) 101, (e) 411, (*f*) 168, (g) 308 and (h) 102. On the Araï plot, open circles indicate the pTRM checks. For each sample, the temperature interval considered for field intensity calculations ($s = -H_{nat}/H_{lab}$) is indicated by the temperatures on the Araï plot and by thick lines on the others two diagrams.

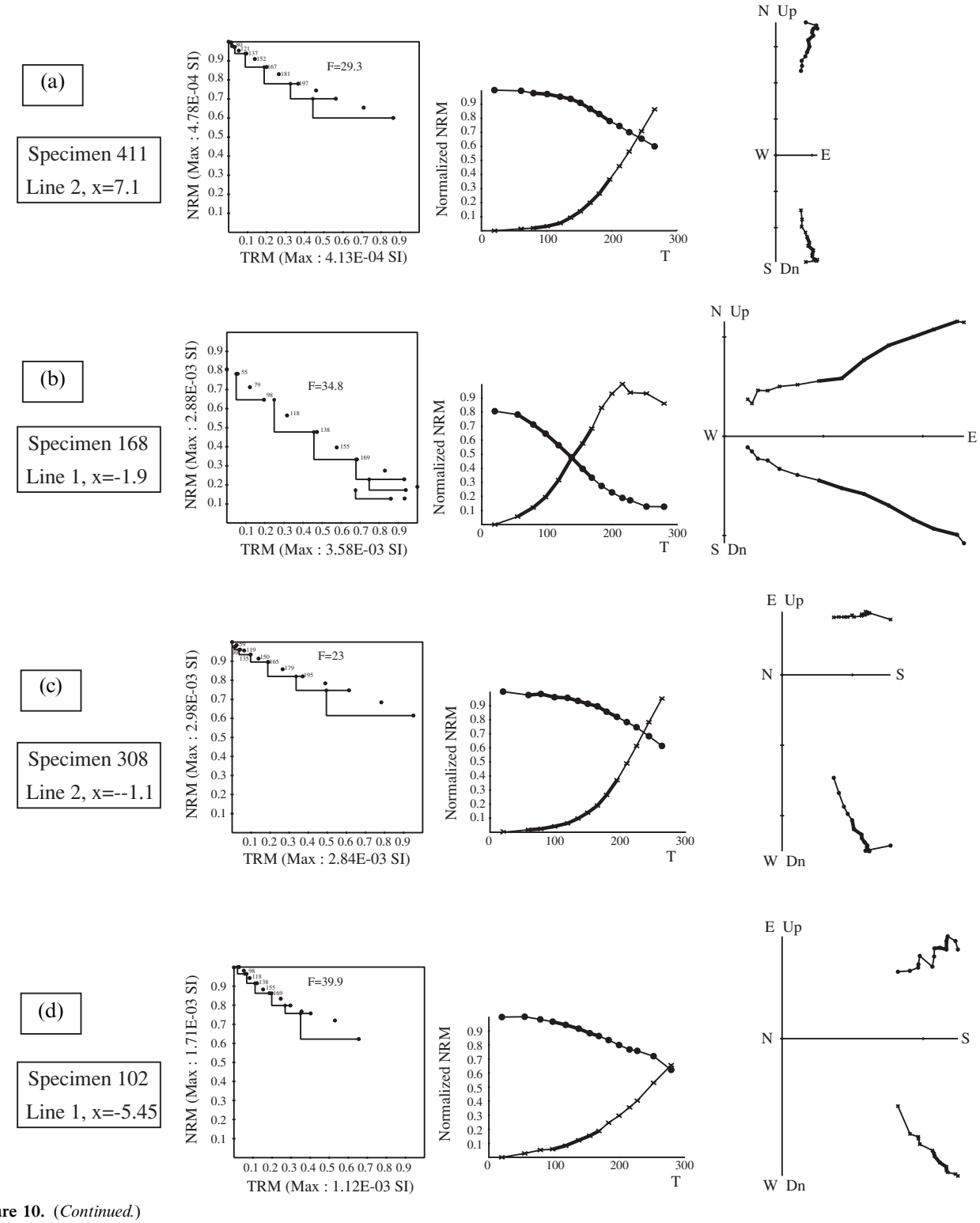

Figure 10. (*Continued.*)

each temperature step, ensuring a temperature reproducibility between the first and the second heatings of a cycle within 1 °C. Moreover, the same heating rate was applied for each paired heating. Due to the large number of samples, cores from Lines 1 (i.e. 26 specimens) and 2 (i.e. 40 specimens) have been treated separately. Both series were performed using temperature increments of 15–20 °C, starting at 55–60 °C and stopping when points clearly began to deviate from a straight line (265 °C for line 1 and 280 °C for line 2) even though appreciable NRM still remains in some specimens.

Palaeointensity data have to satisfy several criteria before being acceptable. Of course, the NRM–TRM plot has to be linear but also only one single component of magnetization has to be present in the temperature interval considered for the

palaeointensity determination. Linearity of the NRM–TRM plot (Fig. 10 left) and the straight segment going through the origin on the orthogonal projections (Fig. 10 right) are evaluated by visual inspection of the diagrams. Furthermore, there should be no significant change of the susceptibility values, measured at room temperature after each heating, within the considered temperature interval, and the pTRM checks have to be positive. The quality of a palaeointensity value is commonly estimated by the quality factor q (Coe *et al.* 1978). However, we preferred to consider separately five parameters to assess the quality of each determination:

(1) a numeric estimate of the coincidence between the pTRM check and the original pTRM,

$$\%\mathrm{TRM} = \frac{|\mathrm{pTRM_{check}} - \mathrm{pTRM}|}{\mathrm{NRM_{20\,deg}}};$$

(2) the width of the temperature interval, ΔT;
(3) the number of temperature steps, N;
(4) the fraction of total NRM used for determination, f;
(5) the standard error on the palaeointensity calculation, s.

The arbitrary threshold values assigned to each of these parameters are as follow: pTRM per cent does not exceed 6, ΔT, N and f must exceed 100 °C, 4 and 10 per cent, respectively, and finally s must be less than 10 per cent.

3.4.2 *Experimental results*

Almost half of our collection did not allow palaeointensity determinations. Some specimens have been rejected because of the occurrence of chemical changes during the very first stages of the treatment, as early as 60 °C, evidenced by a deflection of the remanence directions towards the cylindrical axis of the specimens. Other specimens have been excluded either because of the absence of any alignment on the NRM–TRM plots or because of a departure from a straight line resulting in a concave-down tendency. This is often attributed to the presence of multidomain grains (e.g. Levi 1977) and it is interesting to note that these concave-down plots were observed for four of the five specimens (202, 309, 402 and 403) assumed to be in relatively coarser-grained assemblages (see Section 3.1). The observed concave-down tendency can also be explained by a gradual chemical modification (Prévot *et al.* 1983), in agreement with the jointly observed systematic deviation of the pTRM checks. Finally, determinations that pass fewer than four of the five criteria described above (i.e. pTRM per cent, ΔT, N, f and s) are systematically rejected. A grade 'A' is ascribed to a specimen fulfilling the five criteria, and a grade 'B' if only four criteria are passed.

As the viscosity of the samples was very low, the minimum temperature used for the accepted determinations (Table 3) is taken from between room temperature and 100 °C, while the upper temperatures range from 100 to 265 °C. An increase in TRM capacity is a common feature of basaltic rocks when heated, often attributed to the inversion of the original titanomaghemite. This inversion, occurring at temperatures that are z-dependent (see Section 3.3.1) leads, in all cases, to a multiphase mixture. The end product seems to preserve the original remanent magnetization direction but not its intensity as it is several times as magnetic as the original titanomaghemite (e.g. O'Reilly 1984). The remanent magnetization acquired by this new phase results in a change of the NRM/TRM ratio (e.g. Grommé *et al.* 1979). For $\approx$50 per cent of the accepted NRM–TRM diagrams of the Tammar collection, inversion is evidenced by a quite abrupt flattening of the slope between 170 and 220 °C (Figs 10e–h). There is a systematic coincidence between these samples and those that show several magnetic phases during the low-field susceptibility measurements. The inversion temperatures observed during the Thellier experiments are about 50 °C lower than those estimated from k–T curves. This discrepancy is most probably accounted for by the different duration of both types of experiments: k–T experiments require short heating–cooling cycles (about 3 hr), whereas Thellier experiments necessitate long and successive stepwise heating–cooling cycles (see Section 3.4.1). The inversion temperature (T_{inv}) dictates the upper temperature used to determine palaeointensity (T_{max}). Two major types of NRM–TRM diagrams were observed depending on the alteration degree. For relatively fresh specimens (Figs 10a–d), only one NRM–TRM line segment is observed and a major fraction of the NRM is used for field intensity determination. If the original magnetic carrier is actually a slightly non-stoichiometric TM, inversion probably occurs but in the last stage of heating (i.e. about 250 °C) when only a minor NRM fraction remains. Conversely, for moderately or highly altered specimens, two NRM–TRM line segments are observed (Figs 10e–h). The first straight line associated with low temperatures probably corresponds to the thermal demagnetization of the original NRM while the second is related to the inversion product and has, therefore, no geomagnetic significance.

34 palaeointensities passing through quality criteria adopted in Section 3.4.1 were obtained from the Tammar samples, with 30 grade 'A' and four grade 'B' (Table 3). They range from 15 to 62 μT. 31 correspond to specimens with 'pseudo-ages' between 0 and 0.8 Myr and three to specimens between 1 and 1.5 Myr old. TRM acquisition is an instantaneous process that records the small-scale temporal variation of the geomagnetic field such as the secular variation. A large dispersion of the results is therefore expected for samples covering a time interval from 0 to $\approx$1.5 Myr. However, other factors also scatter the results. Specimen 606 displays a very high field intensity (62 μT) compared to the other values, despite an excellent analytical precision ($f = 64$ and $q = 57$). Prévot *et al.* (1983) have also obtained high field intensity values from MAR basalts and interpreted them as overestimated because the maghemitization index progressively increases during heating. It seems likely that specimen 606 is affected by a similar chemical process, and the corresponding field intensity should therefore be considered with caution.

Alteration of the Tammar samples is variable. As previously seen, the uppermost temperature to determine a palaeointensity (T_{max}) depends on the inversion temperature (T_{inv}), which decreases for increasing alteration degree of the specimen. On the other hand, the increase in T_{c} resulting from the alteration process is associated with a similar increase of the blocking temperatures (T_{b}). Parameters used for field determinations such as T_{max} and f are most probably controlled by a balance between the opposite trends of T_{inv} and T_{b} with the alteration degree of the specimen. No clear variation is seen on T_{max} or f plots as a function of the distance to the ridge axis (Figs 11a and b), in agreement with the absence of systematic fluctuations in the distribution of T_{c} (see Section 3.3.3 and Fig. 9a). Similarly, T_{max} and f show no clear relationship with

Table 3. Results of palaeointensity determinations. From left to right (columns 1–18): 1, 2 sample label and location; 3, 4, 5 rock magnetic properties with hysteresis ratios and T_c; 6, 7 field intensity (μT) and corresponding VADM (10^{22} A m^2); 8–13 five criteria considered for addressing the quality of the determination and corresponding grade (see text); 14–18 other criteria: gap factor (*g*), slope (*b*) and standard error (*db*), quality factor (*q*) and dispersion parameter (Kappa).

No	*Po* km	J_{rs}/J_s	H_{cr}/H_c	T_c	*F* mT	VADM 10^{22} A m^2	pTRM %	ΔT	*N*	*f*	*s* %	grade	*g*	*b*	*db*	*q*	Kappa
806	−13.5	0.77	1.14	290*	30.5 + /0.6	6.64	2	196 (20–216)	11	40	2	A	0.88	0.61	0.01	18	2018
114	−9.1				28 ± 0.4	6.1	2	164 (20–184)	9	41	1	A	0.87	0.56	0.01	28	2891
802	−8.2	0.74	1.11	240*	22.6 ± 0.9	4.92	3	145 (55–200)	9	41	4	A	0.86	0.45	0.02	9	1951
108	−8.1	0.73	1.17	255*	16.3 ± 0.4	3.55	2	145 (55–200)	9	38	2	A	0.87	0.33	0.01	15	739
801	−7.85	0.13	2.75	180	34.1 + /1.2	7.43	4	98 (20–118)	5	15	4	B	0.74	0.68	0.02	3	1279
104	−6.5	0.71	1.19	265*	30.4 ± 0.5	6.62	5	208 (20–228)	12	62	2	A	0.9	0.61	0.01	34	1131
103	−5.6	0.71	0.98		42.7 ± 1.2	9.3	5	149 (79–228)	10	36	3	A	0.87	0.85	0.02	11	3430
102	−5.45	0.73	1.23	380*	39.9 ± 1.7	8.69	1	71 (98–169)	5	10	4	B	0.75	0.8	0.03	2	5931
101	−5.4	0.57	1.09	215	42 ± 0.3	9.15	2	118 (98–216)	8	47	1	A	0.85	0.84	0.01	51	856
168	−1.9	0.57	1.24	160	34.8 ± 1.3	7.58	6	114 (55–169)	7	55	4	A	0.83	0.7	0.03	12	2630
167	−1.6	0.54	1.21	200	41.1 ± 0.9	8.95	6	233 (20–253)	13	69	2	A	0.91	0.82	0.02	28	1449
166	−0.85				37.7 ± 0.4	8.21	3	71 (98–169)	5	22	1	B	0.74	0.75	0.01	15	1334
161	0.2	0.48	1.41	195	51.4 ± 2	11.2	1	78 (20–98)	4	28	4	B	0.66	1.03	0.04	5	5648
711	1.1				15 + /0.4	3.27	1	161 (55–216)	10	58	3	A	0.88	0.3	0.01	19	584
712	1.5				25.2 + /0.8	5.49	1	114 (55–169)	7	28	3	A	0.81	0.5	0.02	8	3123
713	1.7	0.51	1.26		22.7 ± 1	4.95	2	114 (55–169)	7	65	4	A	0.83	0.45	0.02	12	2094
714	2.4	0.49	1.24	310*	24.2 ± 1	5.27	2	114 (55–169)	7	22	4	A	0.83	0.49	0.02	4	3360
715	2.6	0.65	1.09	250*	31.8 ± 0.6	6.93	4	198 (55–253)	12	34	2	A	0.89	0.64	0.01	15	1442
703	16.9	0.76	1.12		15.5 ± 0.5	3.38	2	129 (55–184)	8	16	3	A	0.83	0.31	0.01	4	5917
702	17.8	0.73	1.15		18.8 ± 0.3	4.1	4	196 (20–216)	11	46	2	A	0.89	0.38	0.01	24	1412
601	−8.1				18.3 ± 0.5	3.99	1	166 (61–227)	11	19	3	A	0.89	0.37	0.01	6	5573
602	−6.8				32.3 ± 1	7.04	1	120 (61–181)	8	10	3	A	0.83	0.65	0.02	3	4101
606	−5.2	0.5	1.37		62.3 ± 0.6	13.6	2	127 (100–227)	9	64	1	A	0.85	1.25	0.01	57	1282
313	−2.1				23.2 ± 0.5	5.05	2	166 (61–227)	11	48	2	A	0.9	0.46	0.01	22	3237
312	−2.1	0.7	1.03	230	27.1 ± 0.5	5.9	4	166 (61–227)	11	72	2	A	0.88	0.55	0.01	38	1438
308	−1.1	0.75	1.08		23 ± 0.9	5.01	1	136 (59–195)	9	16	4	A	0.82	0.46	0.02	3	6634
305	−0.9				23.9 ± 0.3	5.21	3	152 (60–212)	10	74	1	A	0.88	0.48	0.01	58	977
304	−0.1	0.61	1.29		48.2 ± 0.6	10.5	2	186 (60–246)	12	66	1	A	0.91	0.96	0.01	52	8002
303	−0.1				47.9 ± 1.1	10.4	1	185 (61–246)	12	39	2	A	0.9	0.96	0.02	16	10651
301	0.5				38.1 ± 0.4	8.3	2	205 (61–266)	13	67	1	A	0.9	0.76	0.01	56	2406
207	1.8	0.53	1.26		32.2 ± 0.3	7.01	3	151 (61–212)	10	76	1	A	0.86	0.64	0.01	77	1625
401	2.5	0.7	1.28	310*	31.3 ± 0.8	6.82	1	132 (80–212)	9	29	3	A	0.86	0.63	0.02	10	14788
406	3.5	0.75	1.02		35.5 ± 0.7	7.73	1	150 (59–209)	10	40	2	A	0.87	0.71	0.01	18	4344
411	7.1				29.3 ± 0.6	6.38	1	117 (80–197)	8	20	2	A	0.82	0.59	0.01	7	12930

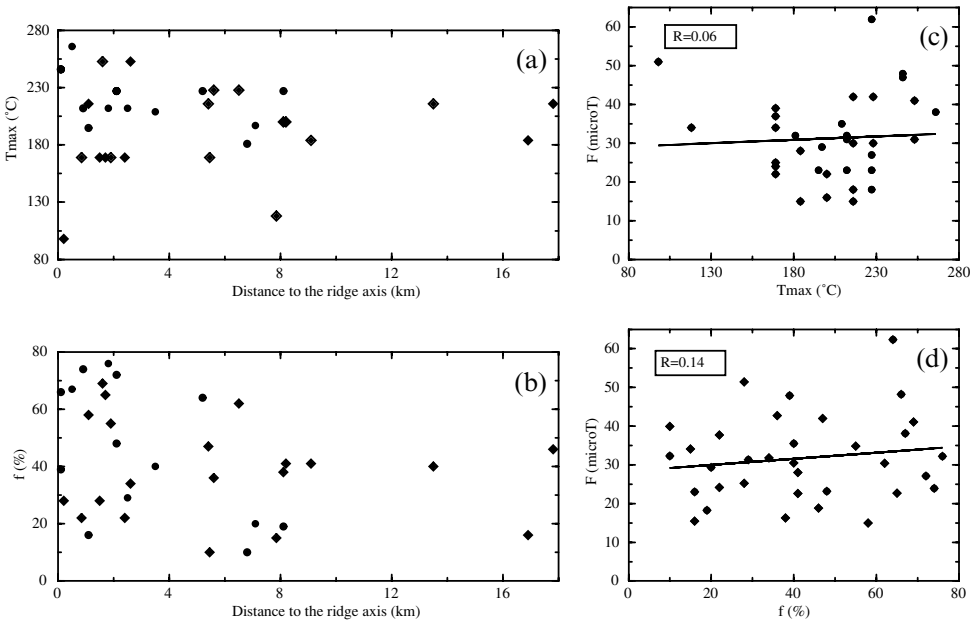

Figure 11. (a) Upper temperature (T_{max}) and (b) fraction of the total NRM (f) used for palaeofield intensity calculation as a function of the distance to the ridge axis. Samples of Line 1 are indicated by circles and those of Line 2 by diamonds. The open symbols surrounding the filled symbols refer to materials collected on the western flank. Palaeofield intensity as a function of T_{max} (c) and f (d). Samples of Line 1 are shown with filled circles and those of Line 2 with filled diamonds.

the palaeofield intensity estimates F (Figs 11c and d). These observations emphasize the absence of a direct link between palaeointensity value and alteration and rule out the possibility of bias due to alteration. Moreover, samples located at the same distance from the ridge axis (i.e. similar age) but displaying different z give similar palaeointensity values. For instance, specimen 101, considered as relatively fresh (Group A, grade 'A'; km 5.4 on the western flank; $f=47$; $T_{max}=216$ °C; $T_c=215$ °C; $z=0.25$), gives a palaeointensity of 42 μT, similar to that of 40 μT obtained from the highly altered specimen 102 (Group B, grade 'B'; km 5.45 on the western flank; $f=10$; $T_{max}=170$ °C; 'pseudo-T_c'$=380$ °C; 'pseudo-z'$=0.7$).

3.4.3 Field intensity as a function of the ridge axis and of NRM intensities

Fig. 12(a) displays the palaeointensities measured on Tammar samples as a function of the distance to the ridge axis. All but one (specimen 606, $F=62$ μT) palaeointensity estimation plot within a narrow band whose mean value is close to the present field intensity in the area (36 μT) computed from the IGRF model. Coherent variations are observed up to at least km 10, with quite similar palaeointensities obtained from samples located at the same distance from the ridge axis, and hence erupted at the same time. Beyond km 10, the number of determinations is sparse (3) and from Line 2 only, and no comparison can be carried out. However, two nearby samples give quite similar field intensities: specimen 703 located at km 17 is associated with a 16 μT intensity ($f=16$ per cent), and specimen 702 at km 18 a 19 μT intensity ($f=46$ per cent). The remarkable coincidence between the two lines and the two flanks gives more confidence in the reliability of the palaeointensity results.

In order to compare palaeointensity measurements from different parts of the world, they are usually converted to virtual dipole moments. As our samples are not oriented, our palaeointensities were transformed into Virtual Axial Dipole Moments (VADMs) using the colatitude of the area in the equation of Merrill & McElhinny (1983). The calculated VADMs are listed in Table 3 and range from 3.4 to 13.6×10^{22} A m^2. The most recently erupted samples (that is, collected within the neovolcanic zone, 'pseudo-ages' between 0 and 0.04 Myr) display VADMs from 8.3 to 11.2×10^{22} A m^2 with a mean of 10×10^{22} A m^2. These values are consistent with the archaeomagnetic data, which display a mean field intensity of 8.7×10^{22} A m^2 for the last 10 kyr reaching a maximum intensity of 11.3×10^{22} A m^2 around 3 kyr (see Table 4). For older times, we used the palaeointensity database (Perrin *et al.* 1998) and selected only values obtained using the Thellier method with pTRM checks. Selected values (that is, 147 determinations for the time interval 0–0.6 Ma, no values between 0.6 and 0.8 Ma) have been mainly obtained from Hawaii and La Réunion in the 0–0.2 Ma interval (i.e. 97 determinations) and from Germany for periods older than 0.3 Ma (i.e. 50 determinations). For time interval 0–0.6 Ma, our data give a mean field intensity of 7.5×10^{22} A m^2, very similar to the 8.0×10^{22} A m^2 obtained with the global database (see Table 4). More detailed variations of the field intensity are addressed by calculating means each 100 kyr using these two data sets (Table 4 and Fig. 12b). Results are quite similar except for the period encompassing the time intervals 0.1–0.2 Ma and 0.4–0.5 Ma. The general agreement between our intensity results and this global data set seems to support the reliability of our palaeointensity determinations (Fig. 12b).

As observed by Juarez *et al.* (1998) on older basaltic samples (5–160 Ma), the variations of NRM intensities of the Tammar samples from 0 to 800 ka are very similar to that

Table 4. Comparison between VADMs of Tammar samples (col. 2), VDMs of global database (col. 3) and archaeomagnetic data (col. 4). For Tammar samples, 'pseudo-ages', VADMs and mean VADMs calculated for the time interval considered (col. 1) are reported. For the database, mean VDMs have been calculated using the number (N) of available determinations (see text). For archaeomagnetic data, only the mean field intensity estimated for the first 10 kyr is indicated.

Time interval	Tammar			Database		Archaeo VDM
	pseudo-age	VADM	mean VADM	VDM	N	
	0.01	10.5				8.75
	0.01	10.4				
	0.02	11.2				
	0.04	8.3				
0–<0.1	0.07	8.21	7.76	8.84	69	
	0.07	5.21				
	0.09	5.01				
	0.09	3.27				
	0.12	5.49				
	0.13	4.95				
	0.13	8.95				
0.1–<0.2	0.14	7.01	6.28	8.61	28	
	0.15	7.58				
	0.17	5.05				
	0.17	5.9				
	0.19	5.27				
	0.2	6.82				
0.2–<0.3	0.21	6.93	7.16	7.71	14	
	0.28	7.73				
0.3–<0.4				6.45	2	
	0.41	13.6				
0.4–<0.5	0.43	8.69	10.19	5.99	27	
	0.43	9.15				
	0.44	9.3				
	0.52	6.62				
0.5–<0.6	0.54	7.04	6.68	6	7	
	0.56	6.38				
	0.62	7.43				
0.6–<0.7	0.64	3.55	4.97			
	0.64	3.99				
	0.65	4.92				
0.7–<0.8	0.72	6.1	6.1			
	1.07	6.64				
>1	1.34	3.38	4.71			
	1.41	4.1				
0–1.41		6.9				
0–0.8		7.11				
0–0.6		7.48		8	147	

of the palaeofield strength (Figs 2b and 12a). Low NRM intensities observed at km 1 (i.e. about 80 ka) and km 7–8 (i.e. 560–640 ka) correspond, respectively, to low palaeofield intensities of about 20 and 25 μT, while high NRM intensities at km 3 (i.e. 240 ka) and km 5–6 (i.e. about 440 ka) correspond, respectively, to high field intensities of 30 and 40 μT. A plot of NRM intensities of the Tammar samples versus palaeofield intensities (Fig. 13) displays a clear trend despite a significant scatter ($R=0.59$).

4 DISCUSSION

4.1 NRM intensities more dependent on palaeofield intensity than on alteration

Because of inversion, T_c is difficult to estimate but the defined 'pseudo-T_c' of moderately to highly altered materials seems a fairly good approximation of the true value (see Section 3.3.1). Regarding the rather uniform geochemical composition of the erupted basaltic rocks (Fig. 5) and the observed relationship linking T_c and k (Fig. 8), variations of T_c are assumed to reflect the oxidation degree of the sample. The scatter of T_c with age suggests that oxidation proceeds rapidly during initial magma cooling when promoted by high or moderate temperature, and more slowly on the ridge flanks at 0 °C (e.g. Prévot *et al.* 1981; Kent & Gee 1996).

Therefore, the alteration degree and the NRM intensity of the samples are probably acquired at the ridge axis. No significant discrepancy is observed between the NRM intensities of unaltered and highly altered samples. Despite the quite limited number of points, no obvious relationship ($R=0.48$) links the NRM intensities and the alteration degree estimated using T_c and 'pseudo-T_c' (Fig. 9b). Although the Tammar samples are altered, their NRM intensity does not primarily depend on the oxidation degree. Conversely, the trend observed between palaeofield and NRM intensities (Fig. 13) together with their coincident variations with age (Figs 2b and 12a) suggest that the alternately low and high NRM values are generated by the variations of the palaeofield intensity at the time of acquisition. NRM intensities of the Tammar collection are, at least for specimens giving reliable palaeofield intensity determinations, more dependent on the geomagnetic field intensity at the time of acquisition than on the alteration degree. This leads to a paradox: basalts are moderately to highly altered during the initial magma cooling, with 'pseudo-z' between 0 and 0.7, but provide reliable determination of the palaeofield intensity. An important point to discuss is the type of remanent magnetization included: TRM, chemical remanent magnetization (CRM) or thermochemical remanent magnetization (TCRM).

4.2 Titanomaghemites as accurate field intensity recorders

The end products and the type of remanent magnetization directly depend on the temperature at which alteration occurs, mostly during the initial magma cooling (see Section 4.1). At temperatures as high as 600 °C, deuteritic oxidation leads to a multiphase mixture similar to the product resulting from the low-temperature inversion of the titanomaghemites (Hauptman 1974). The multiphase mixture obtained during some of the k–T experiments (Figs 6c and d) may therefore be interpreted as original magnetic phases. However, the irreversibility of the cooling curves suggests an original titanomaghemite that has generated new magnetic phases in the laboratory as a result of inversion. We consider that the observed T_c and 'pseudo-T_c' range (130–380 °C) characterize a single magnetic phase. As a consequence, magnetization is acquired at a temperature lower than the deuteritic oxidation temperature. The resulting products of original stoichiometric TM oxidation at a temperature above the titanomaghemite inversion temperature are non-stoichiometric TM, followed by a mixture of several original

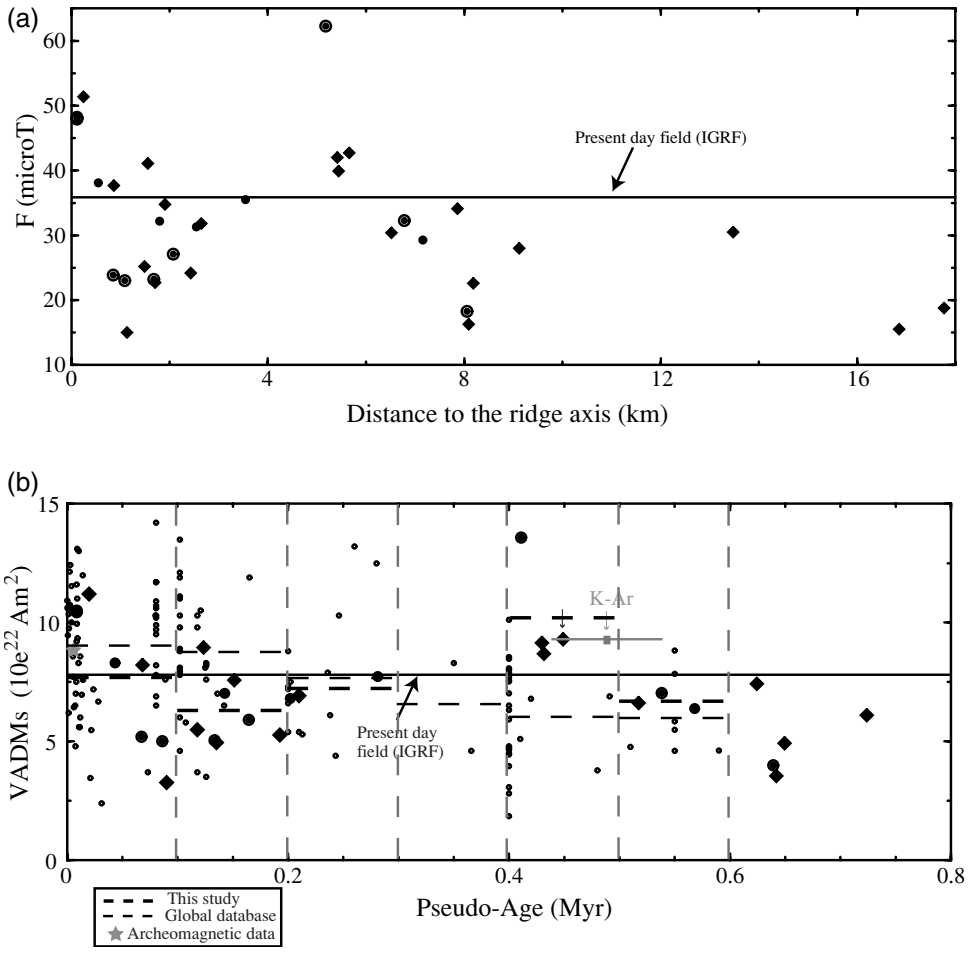

Figure 12. (a) Accurate palaeofield intensities calculated using Tammar materials as a function of the distance to the ridge axis. See Fig. 11(a) for symbols. The present-day field intensity computed at the site by the IGRF is also indicated (black line). (b) Calculated Tammar VADMs for Brunhes chron and selected VDMs extracted from the palaeomagnetic database (small open circles) as a function of the relative age. For comparison, the present-day field intensity computed at the site by the IGRF (black thin line), the mean field intensity for the last 10 kyr given by archaeomagnetic data (grey star) and the mean field intensity calculated each 100 kyr using Tammar samples and the global database (thick and thin dashed lines, respectively) are indicated. The grey line indicates the absolute K–Ar age of sample 103.

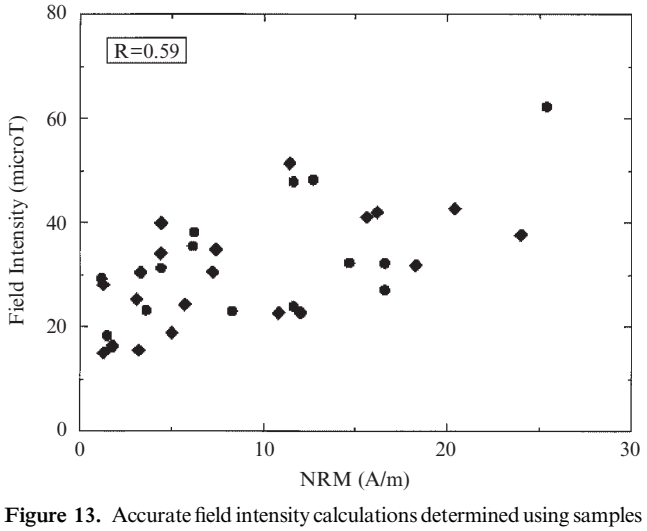

Figure 13. Accurate field intensity calculations determined using samples collected along Line 1 (filled circles) and Line 2 (filled diamonds) as a function of NRM intensities.

magnetic phases. As only one magnetic phase is observed in the samples, alteration indeed occurs at temperatures below the dissociation temperature range of the titanomaghemite. Two different scenarios can be envisaged, either a 'post-TRM maghemitization' (that is, TRM acquisition precedes maghemitization) or a 'pre-TRM maghemitization' (that is, maghemitization precedes TRM acquisition).

In the first scenario, maghemitization occurs at a temperature lower than the T_c of the initial unaltered TM (i.e. about 150 °C), generating non-stoichiometric magnetic particles bearing a CRM. Previous studies suggest that material encountering a 'post-TRM maghemitization' process is suitable for the Thellier experiment up to a threshold non-stoichiometric degree of $z = 0.3$, because the NRM loss remains proportional to the TRM loss; for higher z, Thellier experiments lead to spurious determinations (Grommé *et al.* 1979). Although relying on merely speculative assumptions (samples of group B), estimates of the degree of alteration from the Tammar collection show z-values higher than 0.3 ('pseudo-z' of 0.7 for specimen 102). Whatever their z-value (higher or lower than 0.3), samples of similar ages lead to similar palaeofield intensity estimations.

The inferred secondary CRM seems, therefore, to mimic closely the properties of the initial TRM, even for a pronounced degree of alteration. As reliable palaeofield intensities are recorded from the axis up to at least 0.8 Myr, NRM-bearing particles are magnetically stable. Samples of group B are systematically associated with a wide hysteresis loop, while narrow hysteresis loops correspond to samples of group A (Figs 3 and 6). This suggests that magnetic particle hardness increases with alteration. Such a tendency has already been reported (Day *et al.* 1977) but laboratory experiments performed using synthetic SD TM60 show an abrupt fall of H_c for a degree of alteration exceeding 0.45 (Özdemir & Dunlop 1985). The initial hardening (i.e. z ranging between 0 and 0.45) may explain the memory of the field intensities by moderately altered magnetic particles (i.e. $z<0.45$) but not for a high degree of alteration (i.e. $z>0.45$). This implies that either the degree of alteration of our samples is largely overestimated or highly altered magnetic particles carry another kind of remanent magnetization, able to store durably the field intensity.

The second scenario involves a major part of the alteration occurring between the inversion temperature and T_c of the original TM. Because of the difficulty in determining the inversion temperature of the titanomaghemite, the upper temperature of the 'pre-TRM maghemitization' scenario remains unclear. Experimental studies of the TRM acquired by SD titanomaghemites have shown that whereas the intensity of the 'pre-TRM maghemitization' is lower than for a 'post-TRM maghemitization', its stability increases with increasing maghemitization (Özdemir & O'Reilly 1982) and may explain the storage of the palaeofield intensities by Tammar samples even for a pronounced degree of alteration. It should be mentioned that this 'pre-TRM maghemitization' process is more likely to give reliable Thellier experiments, as these experiments require an original TRM.

4.3 Absolute versus relative palaeointensities

Sedimentary sequences provide a continuous record of the geomagnetic field intensity through time but only relative palaeointensities can be obtained. Calibration of this signal with absolute palaeofield intensities measured on igneous rocks is difficult because of the patchy nature of the absolute palaeointensity database. A usual method is to select arbitrarily a limited part of the sedimentary signal and to calibrate the relative field intensities with selected absolute palaeofield intensity data (e.g. Lehman *et al.* 1996).

The latest sedimentary relative palaeointensity record (Guyodo & Valet 1999) has been calibrated to the Tammar palaeointensity measurements by simple multiplicative adjustment until the two signals display the best visual coincidence for the period 0–50 ka. Note that both sets are kept in their original timescale. Fig. 14 displays the resulting calibrated relative sedimentary palaeointensity signal with the Tammar absolute palaeofield intensities for the Brunhes chron. From the present day to $\approx$0.6 Myr, all but two absolute palaeointensity measurements fit within the minimum and maximum running averages of the sedimentary palaeointensities. Smoothing by running averages provides a means to simulate the effect of the finite width of the neovolcanic zone. A 500 m wide average is sufficient to account for the scatter in age (distance) of the absolute palaeointensities. This gives a 1 km estimation of the neovolcanic zone width in the range of previous estimations (Gente *et al.* 1991; 1997). The too high outlying absolute palaeofield intensity corresponds to specimen 606, whose field calculation has to be considered with caution (see Section 4.2.1). For crust older than 0.6 Myr, the coincidence between the two signals is less clear. Although their variations seem to be consistent, either the palaeofield intensity given by the volcanic samples is underestimated or that by the sediments is overestimated. It

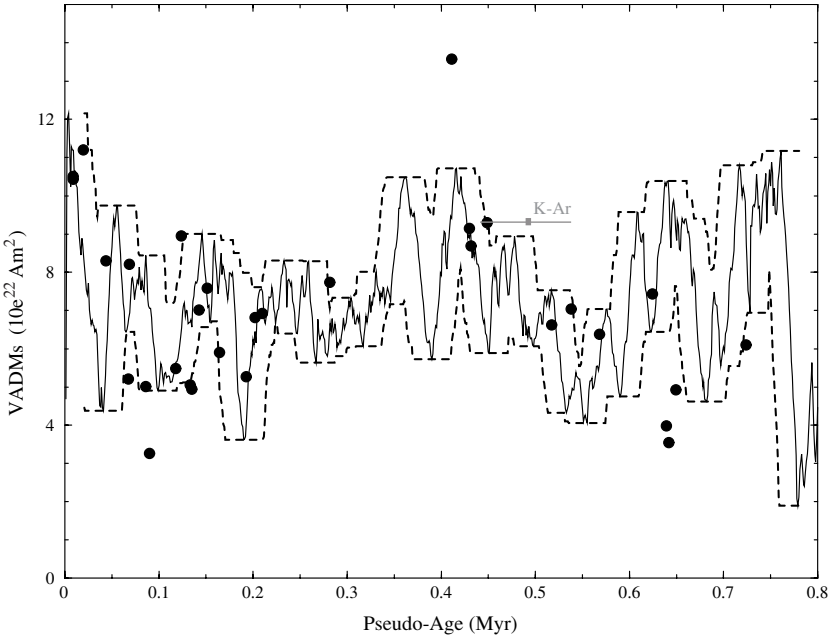

Figure 14. VADMs determined using Tammar samples (filled circles) and the calibrated relative sedimentary palaeointensity record of Guyodo & Valet (1999) (solid line) smoothed by 500 m wide running averages (dashed lines) versus pseudo-age. The grey line indicates the absolute K–Ar age of sample 103.

should be mentioned that the high palaeointensities given by the sedimentary record just after a polarity reversal is vigorously debated, the so-called 'saw-tooth pattern' being attributed either to geomagnetic field behaviour (Valet & Meynadier 1993) or to the process of NRM acquisition in the sediments (Kok & Tauxe 1996a,b; Mazaud 1996).

5 SUMMARY AND CONCLUSIONS

No exponential decay. NRM intensities measured on a large number of samples (66) encompassing a section of oceanic crust 0–1.5 Myr old in the Tammar area do not show the exponential decay with age assumed to characterize maghemitization (that is, decay estimated between 20 and 500 ka) but display quite coherent short-wavelength variations. The effect of grain size, Ti content variability in the TM structure and amount of magnetic minerals are evaluated, but none shows the variations required to generate the observed NRM intensities. Either alteration or field intensity may be responsible for these NRM intensities.

NRM intensities more dependent on field intensity than on alteration degree. k–T experiments and high-field magnetic measurements suggest that magnetic particles are fresh to highly altered SD TM. T_c determination is not straightforward for highly oxidized titanomaghemites, which invert below their T_c. We determine a 'pseudo-T_c' for moderately to highly altered materials using the relationship that links the temperature of the Hopkinson peak with the T_c for the relatively fresh materials associated with reversible k–T curves.

Variations of the 15 estimated T_c values are interpreted as reflecting the degree of non-stoichiometry. T_c show no increasing trend with age, suggesting that oxidation is not age-dependent but occurs during the initial magma cooling when enhanced by moderate temperatures. NRM intensities are therefore mostly inherited from the axis. However, the poor relationship observed between NRM intensities and T_c suggests that NRM intensities do not primarily depend on the alteration degree.

Measurements of the geomagnetic palaeointensity using the Thellier double-heating method have been carried out on the 66 Tammar submarine basalts. 34 samples characterized by a degree of alteration ranging from 0 to 0.7 provide apparently reliable palaeointensities. For fresh or moderately altered materials, the major part of the NRM is thermally demagnetized. Inversely, for more altered materials, less than half of the NRM is thermally demagnetized before chemical modification occurs. Samples of similar age display coincident field intensities whatever the material, fresh or highly oxidized. Variations of NRM intensities with time correlate quite well with that of field palaeointensity, suggesting that NRM intensities are more sensitive to the palaeofield intensity prevailing at the time of NRM acquisition than to the alteration degree.

Titanomaghemites as accurate field intensity recorders. As a consequence of rapid alteration, magnetic carriers are no longer stoichiometric TM, but titanomaghemites. Depending on the alteration temperature, the type of remanent magnetization carried by the resulting non-stoichiometric particles is either a CRM or a TRM or a mixture of both. The reliability of the Thellier experiments suggests that if alteration occurs at a temperature below the T_c of the original magnetic carriers, the resulting CRM closely mimics the initial TRM; conversely, if alteration occurs above the T_c of the original magnetic carriers, the titanomaghemites would not carry a CRM but a TRM. This 'pre-TRM maghemitization' scenario would more convincingly result in successful Thellier experiments and would provide a means for storing a stable record of palaeofield intensity even for a high degree of alteration.

Field intensity variations: a technique to date the oceanic crust? The most recent sedimentary relative palaeointensity signal (Guyodo & Valet 1999) has been calibrated using the absolute palaeointensities determined in this study. The remarkable similarity of both signals strongly suggests that the oceanic basalts indeed record accurately the palaeofield intensity fluctuations. These observations give more confidence in the geomagnetic origin of the 'tiny wiggles' observed on near-bottom magnetic measurements. It may therefore be possible to date accurately the oceanic floor using not only the geomagnetic reversals but also the field intensity fluctuations. Such dating would have a much better resolution than the million years generally obtained with the geomagnetic reversals. The precision of this technique would primarily depend on (1) the steadiness of the spreading process and (2) the width of the neo-volcanic zone. In the Tammar area, the assumption of a 1 km wide steady neo-volcanic zone is consistent with and explains the good record of absolute palaeofield intensities. Such a relative age-dating technique is in agreement with the only absolute K–Ar dating ('Cassignol technique'), which has been successfully performed on one sample.

ACKNOWLEDGMENTS

This study was supported financially by the French programme 'Dorsales' under the 'Appel d'offre ciblé (1997): échelle des temps dans les flux hydrothermaux et magmatiques à l'axe des dorsales'. MR acknowledges research fellowships from the French Ministry of Education and Research. We thank the scientific party of the Tammar cruise, the officers and crew of the R/V Nadir, and the Nautile team for their support during the Tammar cruise. We are thankful to the University of Montpellier II (France), laboratory of Saint-Maur (Paris, France) and Ecole Normale Supérieure (Paris, France) for providing the required equipment for Thellier experiments (Montpellier), high-field (Saint-Maur) and k–T (ENS) measurements. We also thank Chie Honsho (Ocean Research Institute, Japan) for providing near-bottom magnetic measurements, Georges Ceuleneer (Observatoire Midi-Pyrénées, Toulouse, France) for geochemical analyses and Sebastien Gac for thermal simulation of pillow lava cooling. We also appreciate the helpful comments of the reviewers, Jürgen Matzka and Lisa Tauxe, and of the journal's reviewers, Heinrich Soffel.

REFERENCES

Akimoto, S., Katsura, T. & Yoshida, M., 1957. Magnetic properties of $TiFe_2O_4$-Fe_3O_4 system and their change with oxidation, *J. Geomag. Geoelectr.,* **4,** 165–178.

Bina, M.M., 1990. Magnetic properties of basalts from ODP Hole 648B on the Mid-Atlantic Ridge near 23°N, *Proc. ODP Sci. Results,* **106/109,** 297–302.

Bleil, U. & Smith, B., 1979. Petrology of magnetic oxides at site 417, in *Init. Repts DSDP,* Vol. 51-52-53, part 2, pp. 1411–1428, eds Donnelly, T. *et al.*, US Govt Printing Office, Washington, DC.

Cande, S.C. & Kent, D.V., 1992. Ultrahigh resolution marine magnetic anomaly profiles: a record of continuous paleointensity variations?, *J. geophys. Res.,* **97,** 15 075–15 083.

Cande, S.C. & Labrecque, J.L., 1974. Behavior of the earth's paleomagnetic field from small scale marine magnetic anomalies, *Nature,* **247,** 26–28.

Chevallier, R. & Pierre, J., 1932. Propriétés magnétiques des roches volcaniques, *Ann. Phys.,* **18,** 383–477.

Coe, R.S., Grommé, S. & Mankinen, E.A., 1978. Geomagnetic paleointensities from radiocarbon-dated lava flows on Hawaii and the question of the Pacific nondipole low, *J. geophys. Res.,* **83,** 1740–1756.

Day, R., Fuller, M.D. & Schmidt, V.A., 1977. Hysteresis properties of titanomagnetites: grain size and composition dependence, *Phys. Earth planet. Inter.,* **13,** 260–267.

Gee, J. & Kent, D.V., 1994. Variations in layer 2A thickness and the origin of the central anomaly high, *Geophys. Res. Lett.,* **21,** 297–300.

Gee, J. & Kent, D.V., 1998. Magnetic telechemistry and magmatic segmentation on the southern East Pacific Ride, *Earth planet. Sci. Lett.,* **164,** 379–385.

Gee, J., Schneider, D.A. & Kent, D.V., 1996. Marine magnetic anomalies as recorders of geomagnetic intensity variations, *Earth planet. Sci. Lett.,* **144,** 327–335.

Gente, P., Mével, C., Auzende, J.M., Karson, J.A. & Fouquet, Y., 1991. An example of recent accretion on the Mid-Atlantic Ridge: the Snake Pit neovolcanic ridge (MARK area, 23°22′N), *Tectonophysics,* **190,** 1–29.

Gente, P. *et al.*, 1997. On- and off-axis investigations on a highly magmatic segment of the Mid-Atlantic Ridge (21°40′N): the Tammar cruise, *Interridge News,* **5,** 27–31.

Gillot, P.Y. & Cornette, Y., 1986. The Cassignol technique for K-Ar dating, precision and accuracy: examples from the late Pleistocene to recent volcanics from southern Italy, *Chem. Geol.,* **59,** 205–222.

Grommé, C.S. & Mankinen, E.A., 1976. Natural remanent magnetization, magnetic properties, and oxidation of titanomagnetite in basaltic rocks from DSDP leg 34, in *Init. Repts DSDP,* Vol. 34, pp. 485–494, eds Hart, S.R. & Yeats, R.S., US Govt Printing Office, Washington, DC.

Grommé, C.S., Mankinen, E.A., Marshall, M. & Coe, R.S., 1979. Geomagnetic paleointensities by the Thelliers' method from submarine pillow basalts: effects of submarine weathering, *J. geophys. Res.,* **84,** 3553–3575.

Guyodo, Y. & Valet, J.P., 1999. Global changes in intensity of the earth's magnetic field during the past 800 kyr, *Nature,* **399,** 249–252.

Hauptman, Z., 1974. High temperature oxidation, range of non-stoichiometry, and Curie point variation of cation deficient titanomagnetite $Fe_{2.4}Ti_{0.6}O_4$, *Geophys. J. R. astr. Soc.,* **38,** 29–47.

Honsho, C., Dyment, J., Ravilly, M. & Gente, P., 1997. Surface and near-bottom magnetic study on the Mid-Atlantic ridge segment at 21°40′N, *EOS, Trans. Am. geophys. Un.,* **78,** 693.

Honsho, C., Dyment, J., Gente, P. & Tamaki, K., 1999. Near-bottom magnetic study in the Mid-Atlantic ridge segment at 21°40′N, *J. Conf. Abstract Vol., EUG,* **4,** 391.

Horen, H. & Fleutelot, C., 1998. Highly magnetised and differentiated basalts at the 18°–19°S propagating spreading centre in the North Fiji Basin, *Mar. geophys. Res.,* **20,** 129–137.

Hussenoeder, S.A., Tivey, M.A., Schouten, H. & Searle, R.C., 1996. Near-bottom magnetic survey of the Mid-Atlantic Ridge axis, 24°–24°40′N: implications for crustal accretion at slow-spreading ridges, *J. geophys. Res.,* **101,** 22 051–22 069.

Irving, E., 1970. The mid-Atlantic ridge at 45°N, XIV, oxidation and magnetic properties of basalts; review and discussion, *Can. J. Earth Sci.,* **7,** 1528–1538.

Irving, E., Robertson, W.A. & Aumento, F., 1970. The mid-Atlantic ridge near 45°N, VI, remanent intensity, susceptibility, and iron content of dredged samples, *Can. J. Earth Sci.,* **7,** 226–238.

Johnson, H.P. & Atwater, T., 1977. Magnetic study of basalts from the mid-Atlantic ridge, lat, 37°N, *Geol. Soc. Am. Bull.,* **88,** 637–647.

Johnson, H.P. & Hall, J.M., 1978. A detailed rock magnetic and opaque mineralogy study of the basalts from the Nazca plate, *Geophys. J. R. astr. Soc.,* **52,** 45–64.

Johnson, H.P. & Merril, R.T., 1972. Magnetic and mineralogical changes associated with low-temperature oxidation of magnetite, *J. geophys. Res.,* **77,** 334–341.

Johnson, H.P. & Merril, R.T., 1973. Low-temperature oxidation of a titanomagnetite and the implications for paleomagnetism, *J. geophys. Res.,* **78,** 4938–4949.

Johnson, H.P. & Tivey, M.A., 1995. Magnetic properties of zero-age oceanic crust: a new submarine lava flow on the Juan de Fuca ridge, *Geophys. Res. Lett.,* **22,** 175–178.

Juarez, M.T., Tauxe, L., Gee, S.G. & Pick, T., 1998. The intensity of the Earth's magnetic field over the past 160 million years, *Nature,* **394,** 878–881.

Kent, D.V. & Gee, J., 1994. Grain-size dependent alteration and the magnetization of oceanic basalts, *Science,* **265,** 1561–1563.

Kent, D.V. & Gee, J., 1996. Magnetic alteration of zero-age oceanic basalt, *Geology,* **24,** 703–706.

Klitgord, K.D., 1976. Sea-floor spreading: the Central Anomaly Magnetization High, *Earth planet. Sci. Lett.,* **29,** 201–209.

Klitgord, K.D., Huestis, S.P., Mudie, J.D. & Parker, R.L., 1975. An analysis of near-bottom magnetic anomalies: Sea-floor spreading and the magnetized layer, *Geophys. J. R. astr. Soc.,* **43,** 387–424.

Kok, Y.S. & Tauxe, L., 1996a. Saw-toothed pattern of relative paleointensity records and cumulative viscous remanence, *Earth planet. Sci. Lett.,* **137,** 95–99.

Kok, Y.S. & Tauxe, L., 1996b. Saw-toothed pattern of sedimentary paleointensity records explained by cumulative viscous remanence, *Earth planet. Sci. Lett.,* **144,** E9–E14.

Lehman, B., Laj, C., Kissel, C., Mazaud, A., Paterne, M. & Labeyrie, L., 1996. Relative changes of the geomagnetic field intensity during the last 280 kyear from piston cores in the Açores area, *Phys. Earth planet. Inter.,* **93,** 269–284.

Levi, S., 1977. The effect of magnetic particle size on paleointensity determinations of the geomagnetic field, *Phys. Earth planet. Inter.,* **13,** 245–259.

Marshall, M. & Cox, A., 1971. Effect of oxidation on the natural remanent magnetization of titanomagnetite in suboceanic basalt, *Nature,* **230,** 28–31.

Marshall, M. & Cox, A., 1972. Magnetic changes in pillow basalts due to sea-floor weathering, *J. geophys. Res.,* **77,** 6459–6469.

Mazaud, A., 1996. Sawtooth variation in magnetic intensity profiles and delayed acquisition of magnetization in deep sea cores, *Earth planet. Sci. Lett.,* **139,** 379–386.

McElhinny, M.W. & Senanayake, W.E., 1982. Variations in the geomagnetic dipole; the past 50000 years, *J. Geomag. Geoelectr.,* **34,** 39–51.

Merrill, R.T. & McElhinny, M.W., 1983. *The Earth's Magnetic Field: its History, Origin and Planetary Perspectives,* Academic Press, London.

Moskowitz, B.M., 1981. Methods for estimating Curie temperatures of titanomaghemites from experimental Js-T data, *Earth Plant. Sci. Lett.,* **53,** 84–88.

Néel, L., 1949. Théorie du traînage magnétique des ferromagnétiques en grains fins avec application aux terres cuites, *Ann. Geophys.,* **5,** 99–136.

O'Reilly, W., 1984. *Rock and Mineral Magnetism*, Blackie and Son, Glasgow.

Özdemir, Ö. & Dunlop, D.J., 1985. An experimental study of chemical remanent magnetizations of synthetic monodomain titanomaghemites with initial thermoremanent magnetizations, *J. geophys. Res.,* **90,** 11 513–11 523.

Özdemir, Ö. & O'Reilly, W., 1982. An experimental study of thermoremanent magnetization acquired by synthetic monodomain titanomaghemites, *J. Geomag. Geoelectr.,* **34,** 467–478.

Ozima, M. & Larson, E.E., 1970. Low- and high-temperature oxidation of titanomagnetite in relation to irreversible changes in the magnetic properties of submarine basalts, *J. geophys. Res.,* **75,** 1003–1017.

Perfit, M.R. & Fornari, D.J., 1983. Geochemical studies of abyssal lavas recovered by DSRV Alvin from eastern Galapagos rift, Inca Transform, and Ecuador rift, 2, phase chemistry and crystallization history, *J. geophys. Res.,* **88,** 10 530–10 550.

Perrin, M., Schnepp, E. & Shcherbakov, V., 1998. Updated paleointensity database, *EOS, Trans. Am. geophys. Union,* **79,** 198.

Petersen, N., Eisenach, P. & Bleil, U., 1979. Low-temperature alteration of the magnetic minerals in ocean floor basalts, in *Deep Drilling Results in the Atlantic Ocean: Ocean Crust,* pp. 169–209, eds Talwani, M., Harrison, C.G.A. & Hayes, D.E., AGU, Washington.

Pick, T. & Tauxe, L., 1993. Holocene paleointensities: Thellier experiments on submarine basaltic glass from the east Pacific Rise, *J. geophys. Res.,* **98,** 17 949–17 964.

Prévot, M. & Lecaille, A., 1976. Comments on 'Sea-floor spreading: the central anomaly magnetization high', by K.D. Klitgord, *Earth planet. Sci. Lett.,* **33,** 164–168.

Prévot, M., Lecaille, A. & Mankinen, E.A., 1981. Magnetic effects of maghemitization of oceanic crust, *J. geophys. Res.,* **86,** 4009–4020.

Prévot, M., Mankinen, E.A., Grommé, C.S. & Lecaille, A., 1983. High paleointensities of the geomagnetic field from thermomagnetic studies on rift valley pillow basalts from the mid-Atlantic ridge, *J. geophys. Res.,* **88,** 2316–2326.

Prévot, M., Mankinen, E.A., Coe, R.S. & Grommé, C.S., 1985. The Steens Mountain (Oregon) geomagnetic polarity transition, 2, field intensity variations and discussion of reversal models, *J. geophys. Res.,* **90,** 10 417–10 448.

Readman, P.W. & O'Reilly, W., 1972. Magnetic properties of oxidized (cation-deficient) titanomagnetites (Fe, Ti, $[]$)$_3$O$_4$, *J. Geomag. Geoelectr,* **24,** 69–90.

Ryall, P.J.C. & Ade-Hall, J.M., 1975. Radial variation of magnetic properties in submarine pillow basalts, *Can. J. Earth Sci.,* **12,** 1959–1969.

Shcherbakov, V.P., McClelland, E. & Shcherbakova, V.V., 1993. A model of multidomain thermoremanent magnetization incorporating temperature-variable domain structure, *J. geophys. Res.,* **98,** 6210–6216.

Sinton, J.M., Wilson, D.S., Christie, D.M., Hey, R.N. & Delaney, J.R., 1983. Petrologic consequences of rift propagation on oceanic spreading ridges, *Earth planet. Sci. Lett.,* **62,** 193–207.

Smith, B.M., 1987. Consequences of the maghemitization on the magnetic properties of submarine basalts: synthesis of previous works and results concerning basement rocks from mainly DSDP Legs 51 and 52, *Phys. Earth planet. Inter.,* **46,** 206–226.

Smith-Daignières, B., 1984. Propriétés magnétiques de roches basaltiques provenant de la couche 2 de la croûte océanique. Effets du degré de cristallisation et de l'altération basse température, *PhD thesis,* University of Paris VI, France.

Steiger, R.H. & Jäger, E., 1977. Subcommission on geochronology: convention on the use of decay constants in geo- and cosmochronology, *Earth planet. Sci. Lett.,* **36,** 359–362.

Thellier, E. & Thellier, O., 1944. Recherches géomagnétiques sur des coulées volcaniques d'Auvergne, *Ann. Geophys.,* **1,** 37–52.

Thellier, E. & Thellier, O., 1959. Sur l'intensité du champ magnétique terrestre dans le passé historique et géologique, *Ann. Geophys.,* **15,** 285–378.

Thibaud, R., Gente, P. & Maia, M., 1998. A systematic analysis of the mid-Atlantic ridge morphology and gravity between 15° and 40°N: constraints of the thermal structure, *J. geophys. Res.,* **103,** 24 223–24 243.

Valet, J.P. & Meynadier, L., 1993. Geomagnetic field intensity and reversals during the past four million years, *Nature,* **366,** 234–238.

Vlastelic, I., Dosso, L., Guillou, H., Bougault, H., Géli, L., Etoubleau, J. & Joron, J.L., 1998. Geochemistry of the Hollister ridge: relation with the Lousville hotspot and the Pacific-Antartic ridge, *Earth planet. Sci. Lett.,* **160,** 777–793.

Vogt, P.R. & Johnson, G.L., 1973. Magnetic telechemistry of oceanic crust?, *Nature,* **245,** 373–375.

Zhou, W., Van der Voo, R. & Peacor, D.R., 1997. Single-domain and superparamagnetic titanomagnetite with variable Ti content in young ocean-floor basalts: no evidence for rapid alteration, *Earth planet. Sc. Lett.,* **150,** 353–362.

Zhou, W., Van der Voo, R. & Peacor, D.R., 1999. Preservation of pristine titanomagnetite in older ocean-floor basalt and its significance for paleointensity studies, *Geology,* **27,** 1043–1046.